Journal of Neurochemistry

WILEY

Journal of Neurochemistry JNC The Official Journal of the International Society for Neurochemistry

ORIGINAL ARTICLE OPEN ACCESS

Genetic Markers of Postmortem Brain Iron

Marilyn C. Cornelis[1] | Amir Fazlollahi[2,3] | David A. Bennett[4] | Julie A. Schneider[4] | Scott Ayton[5,6]

[1]Department of Preventive Medicine, Northwestern University Feinberg School of Medicine, Chicago, Illinois, USA | [2]Department of Radiology, Royal Melbourne Hospital, University of Melbourne, Melbourne, Victoria, Australia | [3]Queensland Brain Institute, The University of Queensland, Brisbane, Queensland, Australia | [4]Rush Alzheimer's Disease Center, Chicago, Illinois, USA | [5]The Florey Institute of Neuroscience and Mental Health, Melbourne, Victoria, Australia | [6]Florey Department of Neuroscience and Mental Health, The University of Melbourne, Melbourne, Victoria, Australia

Correspondence: Marilyn C. Cornelis (marilyn.cornelis@northwestern.edu)

Received: 21 October 2024 | **Revised:** 26 December 2024 | **Accepted:** 2 January 2025

Funding: This work was supported by the National Institute on Aging (R01AG054057, R01AG065398, R01AG17917, U01AG46152, U01AG61356).

ABSTRACT

Brain iron (Fe) dyshomeostasis is implicated in neurodegenerative diseases. Genome-wide association studies (GWAS) have identified plausible loci correlated with peripheral levels of Fe. Systemic organs and the brain share several Fe regulatory proteins but there likely exist different homeostatic pathways. We performed the first GWAS of inductively coupled plasma mass spectrometry measures of postmortem brain Fe from 635 Rush Memory and Aging Project (MAP) participants. Sixteen single nucleotide polymorphisms (SNPs) associated with Fe in at least one of four brain regions were measured ($p < 5 \times 10^{-8}$). Promising SNPs ($p < 5 \times 10^{-6}$) were followed up for replication in published GWAS of blood, spleen, and brain imaging Fe traits and mapped to candidate genes for targeted cortical transcriptomic and epigenetic analysis of postmortem Fe in MAP. Results for SNPs previously associated with other Fe traits were also examined. Ninety-eight SNPs associated with postmortem brain Fe were at least nominally ($p < 0.05$) associated with one or more related Fe traits. Most novel loci identified had no direct links to Fe regulatory pathways but rather endoplasmic reticulum-Golgi trafficking (*SORL1, SORCS2, MARCH1, CLTC*), heparan sulfate (*HS3ST4, HS3ST1*), and coenzyme A (*SLC5A6, PANK3*); supported by nearest gene function and omic analyses. We replicated ($p < 0.05$) several previously published Fe loci mapping to candidate genes in cellular and systemic Fe regulation. Finally, novel loci (*BMAL, COQ5, SLC25A11*) and replication of prior loci (*PINK1, PPIF, LONP1*) lend support to the role of circadian rhythms and mitochondria function in Fe regulation more generally. In summary, we provide support for novel loci linked to pathways that may have greater relevance to brain Fe accumulation; some of which are implicated in neurodegeneration. However, replication of a subset of prior loci for blood Fe suggests that genetic determinants or biological pathways underlying Fe accumulation in the brain are not completely distinct from those of Fe circulating in the periphery.

1 | Introduction

The capacity for iron (Fe) to undergo redox cycling is exploited by biology for a host of processes relevant to neuronal tissue, such as oxidative phosphorylation, myelin formation, and neurotransmitter synthesis (Singh et al. 2014; Carocci et al. 2018). Yet, this same chemistry can catalyze oxidative damage, and accumulating evidence implicates brain Fe dyshomeostasis in neurodegenerative diseases such as Alzheimer's disease (AD) and Parkinson's disease (PD; Masaldan et al. 2019; Carocci et al. 2018). Brain Fe increases with aging, but this process is enhanced and correlated with clinical deterioration in AD

Abbreviations: ACC, anterior cingulate cortex; AD, Alzheimer's disease; Aβ, amyloid-β; CoA, coenzyme A; DLPFC, dorsal lateral prefrontal cortex; DNAm, DNA methylation; Fe, iron; FPKM, fragments per kilobase of transcript per million fragments mapped; GWAS, genome-wide association study; H3K9ac, histone H3 acetylation on lysine 9; ICP-MS, inductively coupled plasma mass spectrometry; IDP, imaging-derived phenotype; ITC, inferior temporal cortex; MAP, Rush Memory and Aging Project; MFC, mid-frontal cortex; MRI, magnetic resonance imaging; NBIA, neurodegeneration with brain iron accumulation; PD, Parkinson's disease; PM, postmortem; QSM, quantitative susceptibility mapping; ROS, Religious Orders Study; SN, substantia nigra; SNP, single nucleotide polymorphism; TIBC, total iron binding capacity; TSP, transferrin saturation percentage; UKB, UK biobank; WGS, whole-genome sequencing.

and PD (Ayton et al. 2017, 2015, 2021; Zhang et al. 2010; Pesch et al. 2019). Fe coexists with amyloid-β (Aβ) plaque, neurofibrillary tangles, and α-synuclein-containing Lewy bodies (Gong et al. 2019; Telling et al. 2017; Chen et al. 2019), and Fe signaling pathways are altered in neurodegenerating and aging brain (Lu et al. 2017; Zhou and Tan 2017). Ferroptosis, an Fe-dependent and nonapoptotic programmed cell-death pathway, has been proposed as a mechanism of neurodegeneration (Masaldan et al. 2019). Finally, the brain-permeable Fe chelator deferiprone markedly accelerates disease progression in clinical trials of PD (Devos et al. 2022) and AD (Ayton et al. 2025) suggesting Fe elevation is an adaptive response to brain injury, or there is functional Fe deficiency in neurodegeneration (e.g., Fe trapped in pathology). At the peripheral level, Fe status lies on a continuum from anemia to depleted iron stores to iron overload and is captured by different indices. Low blood Fe and hemoglobin (anemia) is associated with AD (Kung et al. 2021; Gong, Sun, and Cong 2023) and PD (Rozani et al. 2019; Zuo et al. 2024; Jiménez-Jiménez et al. 2021). Associations between iron overload or other indices of peripheral Fe status with neurodegenerative disease are unclear (Jiménez-Jiménez et al. 2021; Gong, Sun, and Cong 2023).

Fe balance is tightly regulated by Fe uptake, transport, and storage proteins (Vogt et al. 2021). Dietary Fe intakes poorly correlate with biological levels due, in part, to diet measurement error, compensatory mechanisms, health status as well as genetic factors (Vogt et al. 2021; Moksnes et al. 2022; Sorokin et al. 2022; Liu et al. 2021). Knowledge of the latter offers opportunities to efficiently and noninvasively investigate the causal mechanisms linking Fe to neurodegenerative diseases in addition to identifying subgroups of individuals most susceptible to the health consequences of Fe dyshomeostasis. Genome-wide association studies (GWAS) have identified several plausible loci correlated with peripheral levels of Fe (Moksnes et al. 2022; Sorokin et al. 2022; Liu et al. 2021). Few of these loci overlap with established AD or PD loci (Lambert et al. 2013; Jansen et al. 2019; Kunkle et al. 2019), which may argue against a causal role of Fe in these diseases (Gill et al. 2019; Cheng, Zhu, and Zhang 2019; Wang et al. 2020; Lupton et al. 2017; Larsson et al. 2017).

Neurodegeneration with brain iron accumulation (NBIA) is a class of rare neurological diseases with at least 15 causative genes. *CP* (ceruloplasmin) and *FTL1* (ferritin light chain) are the only NBIA genes directly linked to Fe homeostasis while others (*PANK2, COASY, PLA2G6, C19orf12, FA2H, ATP13A2, WDR45, DCAF17, SCP2, GTPBP2, AP4M1, REPS1, CRAT*) are involved in diverse metabolic pathways such as coenzyme A (CoA) production, lipid metabolism, membrane integrity, autophagy, and mitochondrial function (Levi and Tiranti 2019). That NBIA diseases generally do not cause Fe elevation in the periphery (with the exception of aceruloplasminemia) and that genetic disorders of peripheral Fe homeostasis such as hemochromatosis (*HFE*) and beta-thalassemia (*HBB*) are not causes of NBIA further suggest potentially unique genetic factors contributing to Fe accumulation in the brain. The blood-brain barrier (BBB) limits communication of Fe between brain and body which highlights the distinct regulatory mechanisms between these compartments. Unlike systemic circulation, the tight junctions in the BBB prevent paracellular transport of Fe, necessitating active regulation by transporters. Systemic regulation also centers on liver-derived hepcidin affecting ferroportin, whereas the brain uses locally produced hepcidin, which is under distinct regulatory control (McCarthy and Kosman 2015). Taken together, systemic organs and the brain share several Fe regulatory proteins but there likely exist different homeostatic pathways. Indeed, correlations between peripheral and neural Fe levels are weak (Ganz 2013; Singh et al. 2014; Ayton et al. 2015). Magnetic resonance imaging (MRI) signals are influenced by Fe, myelin, and calcium content due to the shifted magnetic susceptibility (χ) of these constituents relative to tissue water (Liu et al. 2015). Quantitative susceptibility mapping (QSM) MRI methods have been developed to estimate magnetic susceptibility (χ) as a surrogate marker of Fe in vivo (Liu et al. 2015; Wang et al. 2022). Wang et al. (2022) recently implemented a QSM processing pipeline to estimate the susceptibility of multiple brain structures in participants of the UK Biobank (UKB) and performed QSM-Fe GWAS. Identified loci overlap with some but not all loci for peripheral Fe.

In the current study, we perform the first GWAS of postmortem (PM) brain Fe using GW typing and inductively coupled plasma mass spectrometry (ICP-MS) measures of PM brain Fe from a subset of Rush Memory and Aging Project (MAP) participants. We implement a multistep integrative strategy to identify loci which leverages other molecular data available for this cohort as well as prior knowledge and published GWAS results.

2 | Methods

Our GWAS discovery sample included MAP participants with Fe measures and whole-genome-sequencing data (MAP-WGS; Figure 1). Single-nucleotide polymorphism (SNP)-Fe associations maintaining $p < 5\times10^{-6}$ in a pooled analysis of MAP-WGS and additional MAP participants with microarray genotyping (MAP-ARRAY) were followed up for replication in published GWAS of other Fe traits. GW significant SNPs $p < 5\times10^{-8}$ and replicated SNPs were mapped to candidate genes which informed targeted cortical transcriptomic and epigenetic analysis of Fe in a subset of MAP participants. Our full MAP-WGS results were also interrogated for significant genes and pathways.

2.1 | Rush Memory and Aging Project (MAP)

MAP began in 1997 and is a community-based open cohort of residents from over 40 retirement communities and senior public housing units in northeastern Illinois. As detailed previously (Bennett et al. 2012), participants are free of known dementia at enrollment and agree to annual clinical evaluations and organ donation at death. Diet collection began in 2004. At the time of this analysis, 2344 participants have been enrolled and 1081 of these have died. An institutional review board of Rush University Medical Center approved the study, and all participants signed an informed consent and anatomical gift act to donate tissue at death. Participants also signed a repository consent to allow their data to be shared for studies of aging and dementia. Brain

autopsies were performed using standard procedures (Bennett et al. 2012). Total concentrations of Fe in the inferior temporal cortex (ITC), mid-frontal cortex (MFC), anterior cingulate cortex (ACC), and cerebellum (all gray matter) were measured in 688 participants using inductively coupled plasma mass spectrometry as described previously (Ayton et al. 2021; Figure 2). These participants were initially selected from 1064 with available diet data for an independent project. DNA used for genotyping was collected from PM brain tissue, whole blood, or lymphocytes. MAP participants self-reporting as non-Hispanic whites underwent WGS as described previously (De Jager et al. 2018). Subsets of MAP participants were also genotyped on the Affymetrix 6.0 or Illumina OmniQuad Express platform. The same QC protocol was applied to each platform dataset as described previously (De Jager et al. 2012). Genotype imputation was performed on the Michigan Imputation Server using 1000G v3 and HRC v1 reference panels. All annotations align with Genome Reference Consortium Human Build 37 (GRCh37).

DNA methylation (DNAm) measures of the dorsal lateral prefrontal cortex (DLPFC; gray matter) at 415848 discrete CpG dinucleotides have been quantified using the Illumina InfiniumHumanMethylation450 bead chip assay (De Jager et al. 2014). Missing methylation levels from any of these QC'd sites were imputed using a k-nearest neighbor algorithm for k = 100 (De Jager et al. 2014). Histone modification measures were generated using H3K9ac (histone H3 acetylation on lysine 9) chromatin immunoprecipitation sequencing. A total of 26384 H3K9ac "domains" were identified by calculating all genomic regions that were detected as a peak in at least 100 of our 669 MAP + ROS (Religious Orders Study) samples (Klein et al. 2019). Expression of 13484 genes has been quantified using RNA-seq on the Illumina HiSeq for samples with an RNA integrity score > 5 and quantity threshold > 5 ug and at an average sequence depth of 90 million reads (Mostafavi et al. 2018). Quantile-normalization was applied to fragments per kilobase of transcript per million fragments mapped (FPKM), followed by batch correction with the Combat algorithm (Mostafavi et al. 2018). Omic assay protocols and QC procedures have been described in detail previously (De Jager et al. 2014; Klein et al. 2019; Mostafavi et al. 2018).

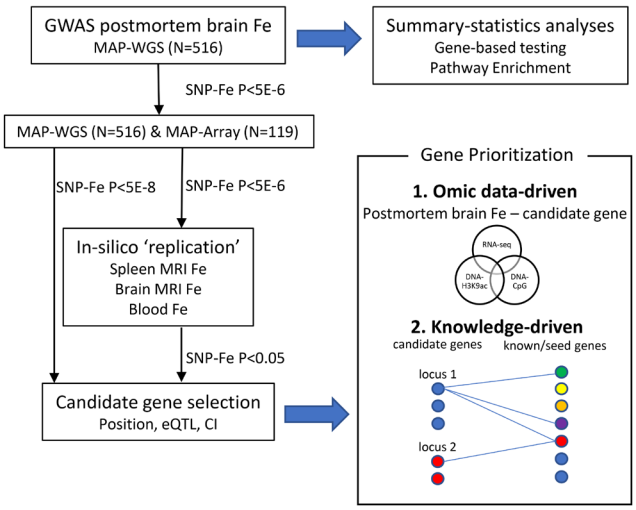

FIGURE 1 | Overview of discovery study design.

2.1.1 | Current Study Sample

Of the 688 MAP participants with PM Fe data, 635 had genetic data (516 with WGS). For the current analyses we excluded 9, 10, 3, and 3 Fe values exceeding four standard deviations of the mean for ITC, MFC, ACC, and the cerebellum,

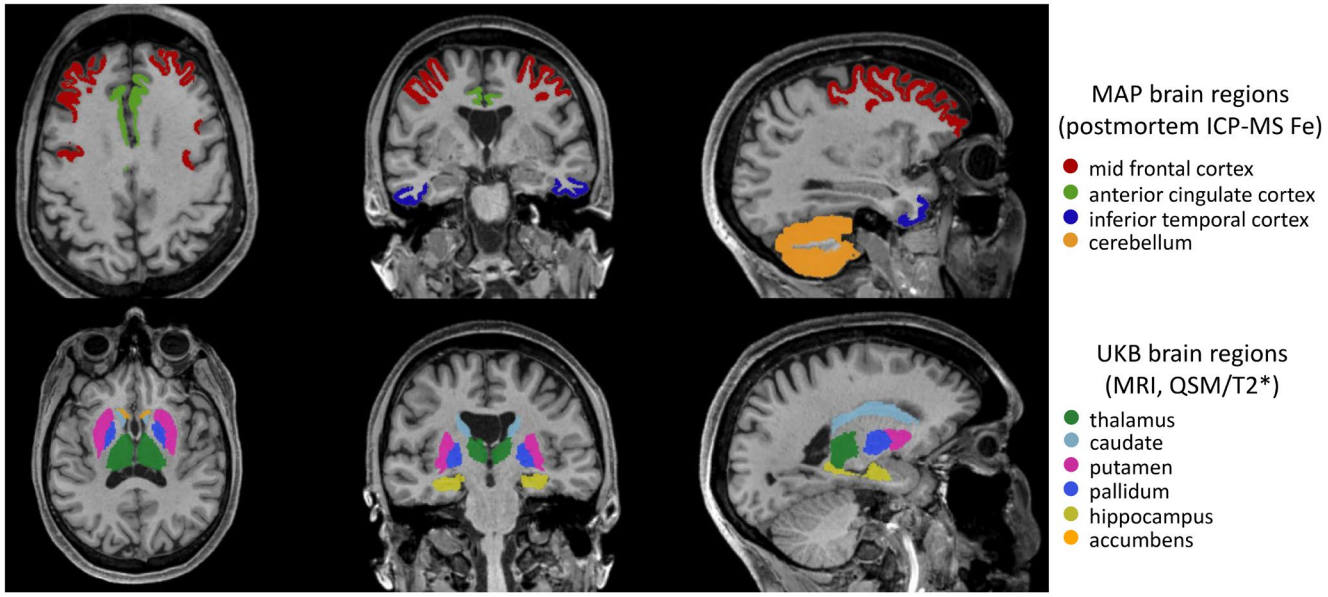

FIGURE 2 | Exemplar image annotating brain regions analyzed in MAP (top panel) and UKB (bottom panel). Amygdala and substantia nigra (UKB) are not annotated.

respectively. Missing values were distributed randomly across regions and participants. Subsets of these 635 participants also had cortical DNAm ($N = 297$), H3K9ac ($N = 283$), and RNA-seq ($N = 286$) data.

2.2 | GWAS Summary-Level Statistics (Table S1)

Summary-levels results for GWAS of brain QSM-Fe and T2*-Fe in UKB were obtained from Wang et al. (2022). The initial UKB sample included 53.1% females aged 45–82 years (64.0 ± 7.5 years) at the time of imaging. Only unrelated British of European ancestry were considered for GWAS. These data included GWAS results for QSM-based (median χ) imaging-derived phenotypes (IDPs) in 16 major subcortical gray matter regions (accumbens, amygdala, caudate, hippocampus, pallidum, putamen, thalamus, and substantia nigra [SN], both left [−L] and right [−R]; Figure 2). Wang et al. (Wang et al. 2022) also derived median T2* measures for SN and re-derived T2* measures for accumbens, amygdala, and hippocampus to account for confounding by macroscopic field gradients. Equivalent T2* for the remaining 8 subcortical regions were derived prior to Wang et al.'s efforts, and while GW significant SNPs were reported (Elliott et al. 2018), full summary-level data for these IDPs were not available for download. For the GWAS, UKB participants were divided into discovery ($n = 19720$) and replication ($n = 9859$) cohorts; two sets of summary-level data were available. Paramagnetic substances (i.e., Fe) and diamagnetic substances (i.e., myelin) have the opposite effect on χ in QSM but the same effect on T2* (Schenck 1996). We obtained GWAS summary-levels results for abdominal MRI-derived spleen-Fe in the UKB ($n = 35324$ British European) as reported by Sorokin et al. (Sorokin et al. 2022). GWAS of abdominal-MRI derived pancreas ($n = 25617$, null) and liver ($n = 32858$) Fe based on the UKB have also been performed (Liu et al. 2021) but summary-level results were not available. GWAS summary-level results for serum iron ($n = 2366120$), ferritin ($n = 257953$), total iron binding capacity (TIBC, $n = 208422$), and transferrin saturation percentage (TSP, $n = 198516$) were obtained from the largest GWAS meta-analysis of Fe status biomarkers to-date involving up to six cohorts of European ancestry including HUNT [median (range) age: 49 (19–103), 53% female], MGI [54 (5–98), 58%], SardiNIA [42 (14–101), 57%], deCODE [44 (0.1–108), 59%], Interval [44 (18–76),50], and DBDS [42 (17–70), 50]; (Moksnes et al. 2022). We used LiftOver as needed to harmonize genomic positions (to GRCh37) across summary-level statistics (Kent et al. 2002).

2.3 | Statistical Analysis

2.3.1 | GWAS of Brain Fe

Our discovery sample consisted of 516 MAP participants with WGS (MAP-WGS). PLINK (Purcell et al. 2007) was used for brain-region specific Fe (μg) GW-analysis using a linear-regression model adjusted for age at death, sex, postmortem interval, and 5 PCs. To maximize sample size and given uncertain causal direction (Fe → AD or AD → Fe) we did not exclude or adjust for AD at death in our primary analysis. ITC and MFC are markedly affected by AD neuropathology while cerebellum is relatively spared (Trejo-Lopez, Yachnis, and Prokop 2022); a key rational for why we performed region-specific GWAS. A preliminary GWAS of a composite measure (Z-score) of Fe that combined all four regions generally weakened or masked associations observed in brain region-specific GWAS and thus was not pursued further. Only di-allelic SNPs with MAF > 1% associated with a trait based on a sample size greater than 468 (> 90% non-missing) were retained in the final summary statistics for genome-wide plots, gene-based testing, enrichment analysis, and replications. When finalizing the final manuscript, we discovered that our initial GWAS included a duplicate (516 individuals but 517 genome-scans). A sensitivity analysis excluding the duplicate produced similar results. Our sample size provided insufficient power to yield meaningful measures of SNP heritability (h^2_{SNP}) and cross-trait genetic correlations (r_g). For example, mean χ^2 values for h^2_{SNP} were too small (e.g., < 1.02), and r_g were not significant with heritability z-scores < 4 (Bulik-Sullivan et al. 2015).

2.4 | Gene-Based, Functional Enrichment, and Pathway Analyses

We performed gene-based association testing for Fe in FUMA (Watanabe et al. 2017, 2019), with MAGMA (de Leeuw et al. 2015), using the matched-ancestry 1000G v3 panel as linkage disequilibrium (LD) reference. Input SNPs were mapped to 20227 protein-coding genes. Significant genes were defined as $p = 0.05/20227 = 2.47 \times 10^{-6}$. MAGMA gene-set analysis was performed for curated gene sets and GO terms obtained from MsigDB, correcting for gene size, variant density, and LD within and between genes. We also used MAGMA to test the association between gene-set properties and tissue-specific gene expression profiles using GTEx (v.7) data from 53 tissues.

2.5 | SNP-Selection, Conditional Analysis, and Sensitivity Analysis

All lead SNP-trait associations maintaining $p < 5 \times 10^{-6}$ in a pooled analysis of MAP-WGS ($n = 516$, excluding duplicate) and MAP-Array ($n = 119$) were taken forward for replication in datasets of related Fe traits and bioinformatic characterization. Independent SNPs were identified by filtering on LD ($r^2 > 0.1$); the most significant (lead) SNP per locus was retained. We identified potentially independent GW significant lead variants by re-running regressions conditioning on the lead SNP from each locus. In sensitivity analysis, we adjusted for supplemental Fe use, dementia status, and history of stroke, heart disease, and hypertension.

2.6 | Reciprocal SNP-Level "Replication"

Lead SNPs identified in GWAS of PM Fe (see above) were followed up for associations with spleen, blood, T2*, and QSM measures of Fe in available summary-statistics for each. Results for SNPs previously associated with the same traits (and liver Fe) in GWAS ($p < 5 \times 10^{-8}$ or publication-defined threshold) were extracted from our final discovery summary statistics (Figure S1). Replication for candidate SNP-trait associations was defined as $p < 0.05$ regardless of effect direction. For QSM/T2*

results (Wang et al. 2022), this threshold applied to Wang et al.'s Discovery sample but additionally required directional consistency in the Replication sample.

2.7 | Candidate Gene Selection

Genes were selected for PM Fe-SNP associations with (i) $p < 5 \times 10^{-8}$ or (ii) $p < 5 \times 10^{-6}$ and replication ($p < 0.05$). Using FUMA (Watanabe et al. 2017, 2019), protein-coding genes were mapped if they were located within 10 kb of the index variants or if annotated to the gene based on cis-eQTL (LD ≥ 0.8), chromatin interaction (CI, LD ≥ 0.8), or methylQTL (LD ≥ 0.8) data from human brain (Westra et al. 2013; GTEx Consortium 2017; Ng et al. 2017; Ramasamy et al. 2014; Wang et al. 2018; Kang et al. 2011). For loci with no candidate genes meeting the former criteria, the closest gene up- and downstream of the index variant were selected as lower-tiered genes. We also present top genes selected by V2G as an alternate gene prioritization method that is non-tissue specific and further integrates functional predictions (Ghoussaini et al. 2021).

2.8 | Candidate Gene Prioritization

2.8.1 | Data-Driven Approach

DLPFC DNAm, H3K9ac, and RNAseq features (independent variables) were mapped to selected candidate genes for association with PM brain Fe levels (dependent variable) in MAP using R or SAS (version 9.1; SAS Institute, Cary, NC) adjusting for at least age at death, sex and postmortem interval. Only candidate genes with non-zero brain expression in >80% of the larger ROSMAP sample were considered. All CpGs (DNAm) within 100 kb of the start/stop positions of each candidate gene were tested with linear regression further adjusting for cross-correlation. All H3K9ac domains within 100 kb of the start/stop positions of each candidate gene were tested with linear regression further adjusting for batch. RNAseq combat-adjusted FPKM values for each candidate gene were tested with linear regression further adjusting for RNA integrity score, log2[total aligned reads], and number of ribosomal bases. For targeted analyses of H3K9ac and RNAseq, statistical significance was defined as $\alpha = 0.05$. For DNAm, p-values of all CpGs per gene were first meta-analyzed into a single observed test statistic using Fisher's method (Brown 1975; Cinar and Viechtbauer 2022) and then a Bonferroni correction was applied for the number of CpGs tested per candidate gene ($\alpha = 0.05/\#\text{CpG}$). Overall declaration of strong supporting molecular evidence required at least two omic-measures to converge.

2.8.2 | Knowledge-Driven Approach

Manual curation of the literature was further facilitated by constructing protein–protein interactions using STRING (Szklarczyk et al. 2021). For the latter, we combined our list of selected candidate genes with "seed" genes obtained from curated pathways related to iron and ferroptosis (Table S2; Subramanian et al. 2005; Liberzon et al. 2011, 2015).

The same candidate gene selection and prioritization pipeline was also applied to replicated published SNPs (Figure S1).

3 | Results

3.1 | GWAS

Table 1 presents the characteristics of MAP participants. Fe across brain regions was significant ($p < 0.0001$) but weakly correlated (r range: 0.14–0.30). Population stratification had negligible effects on GWAS results based on review of quantile-quantile plots (Figure S2) and λgc (range: 1.00–1.02). Our discovery of PM Fe GWAS yielded GW significant loci for ACC (1 locus), MFC (2), ITC (9), and cerebellum (4; $p < 5 \times 10^{-8}$; Table 2, Figures S3 and S4). Conditional analysis did not yield additional independent loci. Gene-based testing yielded 5 significant protein-coding genes ($p < 2.47 \times 10^{-6}$) for MFC Fe (*SPNS3, ABHD14A, ACY1, PCBP4, RRP9*); spanning two regions with SNPs taken forward for replication. A look-up of fifteen NBIA genes all yielded non-significant tests ($p > 0.03$). No significant functional or pathway enrichment was observed across traits. Results for look-ups of prior loci for Fe-implicated neurodegenerative diseases (AD, PD, and multiple sclerosis [MS]) are presented in Tables S3–S5.

3.2 | Reciprocal SNP-Level "Replication"

MAP-WGS yielded a total of 212 independent SNP-trait associations with $p < 5 \times 10^{-6}$ for at least one of the four PM Fe traits. Of these 212 SNPs, 184 were available in MAP-ARRAY and of these, 137 SNPs maintained $p < 5 \times 10^{-6}$ in a pooled analysis of MAP-WGS and MAP-Array. Thus, a total of 165 SNPs (28 unique to WGS) were taken forward for replication in summary-level GWAS of related Fe traits (Table S6). Ninety-eight SNPs were at least nominally associated with one or more related Fe traits (Table S7). In sensitivity analyses adjusting for supplemental Fe use, dementia status, and history of stroke, heart disease, and hypertension, PM Fe associations with 5 SNPs (rs79518659, rs76754208, rs116999652, rs143762891, rs145903584) attenuated remarkably (P difference $> 1 \times 10^{-4}$). SNPs previously associated with related Fe traits in GWAS were extracted from our MAP-WGS GWAS of PM Fe. Candidate SNP-trait associations ($p < 0.05$) are presented in Table S8.

3.3 | Candidate Gene Selection and Prioritization for Novel PM Fe Loci

A total of 209 candidate genes (178 expressed in the brain) were selected for PM Fe-SNP associations with (i) $p < 5 \times 10^{-8}$ or (ii) $p < 5 \times 10^{-6}$ and at least nominal associations with other Fe traits (Table S7). Here, we focus on the most promising novel loci and corresponding prioritized candidate gene inferred by replication, ROSMAP omic results, and biological plausibility (Table 3). A look-up of these loci in the GWAS catalog yielded no overlapping trait associations in LD ($r^2 > 0.8$). For the majority of our candidate genes, we observed inverse associations between H3K9ac and PM Fe; whether this is a function of genes selected

TABLE 1 | Characteristics of MAP participants at time of death.[a]

Characteristic	MAP ($n=635$)
Age at death, years	90.4 ± 6.0
Male, *n* (%)	191 (30)
Postmortem interval	8.0 ± 4.8
Dementia, *n* (%)	277 (44)
Alzheimer's dementia, *n* (%)	219 (34)
Hypertension, *n* (%)	578 (91)
Diabetes, *n* (%)	125 (20)
Stroke, *n* (%)	129 (20)
Heart disease, *n* (%)	186 (29)
Fe, μg	
Inferior temporal cortex	51.5 ± 13.9
Mid-frontal cortex	52.9 ± 14.0
Anterior cingulate cortex	26.7 ± 8.1
Cerebellum	53.2 ± 24.5
Whole-genome sequencing data, *n* (%)[b]	516 (81)
DNAm data, *n* (%)[c]	297 (47)
H3K9ac data, *n* (%)[c]	283 (45)
RNA-seq data, *n* (%)[c]	286 (45)

[a]Values are mean ± SD or *n* (%).
[b]Included in discovery GWAS.
[c]Included in candidate gene validation.

or (more likely) a genome-wide pattern will be a focus of an independent report.

3.4 | ER-Golgi Trafficking

Several promising loci map to candidate genes with no established link to Fe, rather they have roles in endoplasmic reticulum (ER)-Golgi trafficking. The rs144916412 A variant at 11q24.1 associated with higher PM MFC Fe ($p<5\times10^{-6}$) was associated with higher QSM accumbens-L ($p<0.05$) and maps to *SORL1*. The GW significant SNP rs76278520 at 4p16.1 for PM cerebellum Fe ($p<5\times10^{-8}$) was not replicated but omic markers inferred significant inverse correlations between *SORCS2* (and *SORL1*) transcription activity and PM Fe. SORCS2 and SORL1 are members of the vacuolar protein sorting 10 (VPS10) domain-containing receptor family (Hermey 2009). *SORCS2* is highly expressed in the brain and functions as a receptor for the precursor forms of NGF and BDNF (Glerup, Nykjaer, and Vaegter 2014; Uhlén et al. 2015). SORL1 interacts with retromer in regulating the recycling of endosomal cargo, including amyloid precursor protein (APP; Caglayan et al. 2014; Andersen et al. 2005; Nielsen et al. 2007; Fjorback and Andersen 2012), and may also play a role in the uptake of ApoE-rich lipoproteins (Taira et al. 2001).

The rs148427669 C variant at 17q22 (*CLTC*) was associated with higher PM ITC Fe ($p<5\times10^{-6}$) associated with higher QSM pallidum-R but also higher T2* hippocampus-R and amygdala-R ($p<0.05$). *CLTC* encodes a heavy chain subunit of clathrin; a protein component of the coated vesicles and pits and facilitates receptor-mediated endocytosis of a variety of macromolecules, including holo- (Fe-bound) transferrin (Tf)/TFRC (Royle, Bright, and Lagnado 2005; Tortorella and Karagiannis 2014; McCarthy and Kosman 2012).

Variants at 1q32.1 (*GOLT1A*), 5p13.3 (*GOLPH3*), 7q22.3 (*SYPL1*), and 11p14.1 (*RAB30*) associated with PM cerebellum Fe ($p<5\times10^{-6}$) were also nominally associated with QSM measures ($p<0.05$). Candidate genes *GOLT1A*, *GOLPH3*, and *RAB30* encode proteins that localize to the Golgi apparatus (GA) and function in Golgi-trafficking and organization (Conchon et al. 1999; Passemard et al. 2019; Zulkefli et al. 2021). Pantophysin is encoded by the nearby candidate *SYPL1* and is an integral membrane protein of small synaptic and cytoplasmic vesicles released from the trans-Golgi network (TGN) in brain and endocrine cells (Haass, Kartenbeck, and Leube 1996).

The variants at 5q21.1 (*ST8SIA4*) and 7q36.3 (*PTPRN2*) were associated with higher PM ITC Fe ($p<5\times10^{-6}$) and also associated with higher QSM caudate/SN and QSM amygdala-L, respectively ($p<0.05$). *ST8SIA4* encodes a glycosyltransferase that resides in the GA and catalyzes the polycondensation of alpha-2,8-linked sialic acid required for the synthesis of polysialic acid (PSA; Angata et al. 2000). PSA specifically synthesized by ST8SIA4 (also by ST8SIA2) binds to and modulates the adhesive properties of neural cell adhesion molecule, neuropilin-2, skeletal muscle alpha-subunit of voltage-gated sodium channel, E-selectin, and lactoferrin (Mindler, Ostertag, and Stehle 2021; Kühnle et al. 2019; Angata et al. 2000). *PTPRN2* encodes phogrin, a transmembrane glycoprotein expressed in dense-core and synaptic vesicles of several neuroendocrine cell types and that plays a role in vesicle-mediated secretory processes (Torii et al. 2005; Nishimura et al. 2009; Cai et al. 2011).

At 4q32.3, the rs139869159 G variant specific to PM ACC Fe ($p<5\times10^{-6}$) was also associated with higher serum Fe, TSP, and QSM SN-R but also higher T2* amygdala-R and accumbens-L ($p<0.05$). The positional candidate gene at this locus, *MARCH1*, encodes a short-lived ubiquitin ligase targeting TFRC, CD86, FAS, and MHC class II proteins, and promotes their subsequent endocytosis and sorting to lysosomes to reduce the immune response (De Gassart et al. 2008; Tachiyama et al. 2011; Fujita et al. 2013; Martin et al. 2022). TFRC transcripts and protein spike early in response to infection but return to basal levels due, in part, to MARCH1 (Martin et al. 2022).

The GW significant variant at 1p34.3 (rs41267275) for PM ITC Fe ($p<5\times10^{-8}$) did not replicate but epigenetic profiles of promising candidate genes *THRAP3* and *TRAPPC3* supported inverse correlations between transcription activity and PM Fe levels. *TRAPPC3* encodes a subunit of the TRAnsport Protein Particle (TRAPP) II complex implicated in late Golgi trafficking and Golgi stress response (Ramírez-Peinado et al. 2017; Passemard et al. 2019). The nuclear protein encoded by *THRAP3* is a transcriptional coregulator and a selective coactivator for CLOCK-BMAL1 (Lee, Hsu, and Tarn 2010; Lande-Diner et al. 2013; see *BMAL1* below).

TABLE 2 | Genome-wide significant associations with postmortem Fe in MAP-WGS (Discovery).

				Anterior cingulate cortex			Cerebellum			Mid-frontal cortex			Inferior temporal cortex		
				Discovery		Pooled[a]	Discovery		Pooled[a]	Discovery		Pooled[a]	Discovery		Pooled[a]
Chr:position	SNP *nearest gene*	EA/OA	EAF	*β* (se)	*p*	*p*	*β* (se)	*p*	*p*	*B* (se)	*p*	*p*	*β* (se)	*p*	*p*
1:36690748	rs41267275 *THRAP3*	T/C	0.04	1.01 (1.36)	0.46	0.36	11.63 (4.16)	0.005	0.007	5.28 (2.35)	0.03	0.05	15.45 (2.41)	3.6E-10	3.4E-10
4:7475163	rs76278520 *SORCS2*	C/G	0.02	1.55 (1.94)	0.42	0.39	33.93 (5.75)	6.6E-9	3.1E-8	0.06 (3.37)	0.98	0.5	1.93 (3.53)	0.58	0.5
5:6653474	rs8192190 *SRD5A1*	G/A	0.04	1.00 (1.27)	0.43	0.46	4.81 (3.89)	0.22	0.11	3.48 (2.22)	0.12	0.2	12.70 (2.27)	3.4E-8	2.0E-8
7:11782632	rs149651036 *THSD7A*	C/A	0.02	3.32 (1.79)	0.06	0.02	15.12 (5.47)	0.006	0.005	12.10 (3.08)	9.80E-5	8.60E-5	22.06 (3.20)	1.7E-11	1.7E-12
7:51818184	rs74970338 *POM121L12, COBL*	T/G	0.01	3.65 (2.16)	0.09	0.1	2.68 (6.66)	0.69	0.67	4.94 (3.76)	0.19	0.26	22.47 (3.98)	2.9E-8	4.0E-8
7:105842968	rs35447353 *NAMPT, SYPL1*	G/A	0.02	−0.58 (1.75)	0.74	0.68	30.20 (5.19)	1.0E-8	3.8E-8	3.53 (3.04)	0.25	0.21	3.51 (3.18)	0.27	0.32
7:137536270	rs79518659 *DGKI*	T/C	0.02	1.82 (1.74)	0.3	0.54	2.24 (5.22)	0.67	0.64	17.03 (2.93)	1.20E-8	3.60E-7	−0.11 (3.42)	0.98	0.54
9:135290447	rs71503143 *CFAP77, TTF1*	A/G	0.01	12.75 (2.27)	3.4E-8	1.6E-7	8.51 (7.17)	0.24	0.21	4.76 (4.07)	0.24	0.23	4.76 (4.27)	0.27	0.32
11:23765278	rs4077357 *CCDC179, LUZP2*	A/G	0.03	1.81 (1.56)	0.25	0.2	1.97 (4.86)	0.69	0.71	14.97 (2.68)	3.70E-8	2.70E-8	5.14 (2.88)	0.08	0.06
11:109323240	rs75195172 *DDX10, ZC3H12C*	G/A	0.01	4.84 (2.34)	0.04	0.04	2.61 (7.19)	0.72	0.69	7.13 (4.07)	0.08	0.09	25.73 (4.12)	9.0E-10	1.5E-10
12:11635721	rs116953561 *PRB2*	G/A	0.07	0.62 (0.95)	0.52	0.36	7.76 (2.89)	0.007	0.006	0.64 (1.65)	0.7	0.66	9.72 (1.68)	1.4E-8	2.7E-9
12:130496751	rs138514823 *TMEM132D*	A/G	0.01	0.84 (2.17)	0.7	0.65	2.68 (6.66)	0.69	0.76	1.94 (3.78)	0.61	0.61	22.80 (3.83)	4.9E-9	3.1E-10

(Continues)

TABLE 2 | (Continued)

Chr:position	SNP *nearest gene*	EA/ OA	EAF	Anterior cingulate cortex			Cerebellum			Mid-frontal cortex			Inferior temporal cortex		
				Discovery		Pooled[a]	Discovery		Pooled[a]	Discovery		Pooled[a]	Discovery		Pooled[a]
				β (se)	*p*	*p*	*β* (se)	*p*	*p*	*B* (se)	*p*	*p*	*β* (se)	*p*	*p*
16:52860453	rs117683562 *CHD9, TOX3*	G/A	0.01	1.95 (2.44)	0.43	0.36	41.56 (7.24)	1.7E-8	6.6E-7	−2.16 (4.24)	0.61	0.66	10.70 (4.42)	0.02	8.4E-5
17:63392730	rs72862451 *AXIN2, RGS9*	C/A	0.03	2.66 (1.40)	0.06	0.06	23.69 (4.17)	2.2E-8	3.2E-8	0.21 (2.48)	0.93	0.98	1.98 (2.56)	0.44	0.55
20:25736887	rs200637389 *ZNF337*	C/A	0.5	1.95 (5.67)	0.73	NA	6.67 (17.39)	0.7	NA	8.11 (9.86)	0.41	NA	−65.40 (9.92)	1.1E-10	NA
X:39274077	rs139806360 *BCOR, MID1IP1*	A/G	0.03	0.70 (1.20)	0.56	NA	5.24 (3.69)	0.16	NA	2.68 (2.09)	0.2	NA	11.93 (2.13)	3.3E-8	NA

Abbreviations: EA, effect allele; EAF, effect allele frequency; NA, not available; OA, other allele.
[a]NA: SNP not available in MAP-Array for pooled analysis.

Variants at 3q26.2 (*SLC7A14*), 11q25 (*B3GAT1*), and 15q26.3 (*SELENOS/VIMP*) associated with higher PM Fe ($p < 5 \times 10^{-6}$) were also associated with higher blood measures of Fe ($p < 0.05$); but no QSM or T2* measures. *SLC7A14* encodes a largely uncharacterized lysosomal cationic amino-acid (i.e., Arg, Lys, His) transporter (Fotiadis, Kanai, and Palacín 2013; Jiang et al. 2023). *B3GAT1* encodes a glucuronyltransferase localized to the GA that is a key enzyme in the biosynthesis of human natural killer-1 (Kizuka, Tonoyama, and Oka 2009) but also recently implicated in Tf glycosylation (Landini et al. 2022). *SELENOS/VIMP* was supported by epigenetic marks and encodes selenoprotein S, a transmembrane protein localized in the ER, and is involved in the degradation and elimination of misfolded proteins (Ye et al. 2004).

3.5 | Heparan Sulfate

Index variants at 16p12.1 (*HS3ST4*) and 4p16.1 (*HS3ST1*) associated with higher PM ITC Fe ($p < 5 \times 10^{-6}$) were nominally associated with higher QSM pallidum-L/SN-R ($p < 0.05$) and lower T2* SN-R ($p < 0.05$), respectively. Both candidates encode sulfotransferases in the GA that generate (the rare) 3-O-sulfated glucosaminyl residues in heparan sulfate (HS; Lawrence et al. 2007). Chains of HS form HS proteoglycans (HSPG) attached to the extracellular matrix or surface of cells, where they can act as receptors for cytokines/growth factors or as co-receptors for signaling complexes (Xu and Esko 2014). HS modulates hepatic hepcidin expression, but studies are conflicting. In mice, impaired HS biosynthesis reduces hepcidin expression leading to Fe accumulation in the liver and serum (Poli et al. 2019). However, exogenous heparins are also strong inhibitors of hepcidin expression and lead to increased serum Fe (Asperti et al. 2019; Poli et al. 2011, 2019). The index SNP rs150042143 T at 3q27.3 associated with higher PM cerebellum Fe ($p < 5 \times 10^{-6}$) was nominally associated with higher serum Fe ($p < 0.05$). Our positional candidate, *FETUB*, has no plausible role in Fe metabolism. V2G prioritized *HRG*, encoding histidine-rich glycoprotein known to bind several ligands such as heme, heparin, HS, thrombospondin, plasminogen, and divalent metal ions (Wakabayashi 2013; Ackermann et al. 2023).

3.6 | Coenzyme A (CoA)

Variants at 2p23.3 (*SLC5A6*) and 5q34 (*PANK3*) positively associated with PM ACC Fe ($p < 5 \times 10^{-6}$) were positively associated with several QSM IDPs ($p < 0.05$). *SLC5A6* encodes a multivitamin transporter that facilitates pantothenate (CoA precursor), biotin, and lipoate uptake in the digestive system and transport across the BBB (Uchida et al. 2015). *PANK3* encodes a pantothenate kinase which catalyzes the phosphorylation of pantothenate, a rate-limiting step in CoA biosynthesis (Uhlén et al. 2015; Dansie et al. 2014).

3.7 | Others

The GW significant rs72862451 C variant at 17q24.1 for higher PM cerebellum Fe ($p < 5 \times 10^{-8}$) was nominally associated

TABLE 3 | Promising loci associated with postmortem brain iron and their prioritized candidate genes.[a]

Locus						Postmortem brain Fe					Blood Fe				Brain MRI		Candidate gene	Candidate gene selection criteria				Data-driven gene prioritization			Knowledge-driven gene prioritization			
Cytogenetic band	Chromosome	Position (GRCh37/hg19)	dbSNP	Effect allele	Effect allele frequency	ACC	MFC	ITC	Cerebellum	Spleen	S-Iron	TSP	Ferritin	TIBC	8 regions, left & right side (16 total, see Figure 2)[b]	4 regions, left & right side (8 total, see Figure 2 and Methods)[b]	Tier 1, tier 2, [tier 3] candidate genes	Positional (+/− 10 kb)	cis-eQTL (brain, blood)	CI (HiC, Brain)	mQTL (brain)	Brain Fe-RNAseq	Brain Fe-DNA-H3K9ac	Brain Fe-DNA-CpG	Fe/Ferroptosis pathway (direct/seed gene)[c]	STRING (all data types, confidence > 0.7) (indirect)[d]	STRING (experiments confidence > 0.4) (indirect)[d]	Proposed Pathway
1p34.3	1	36 690 748	rs41267275	T	0.04												THRAP3						MFC, ITC	MFC	N	0	0	Circadian
																	TRAPPC3						MFC	MFC	N	0	0	ER-Golgi trafficking
1q32.1	1	204 170 005	rs72749751	T	0.05										1		GOLT1A						MFC, ITC		N	0	0	ER-Golgi trafficking
3q26.2	3	170 356 821	rs116612225	A	0.01												[SLC7A14]						ITC		N	0	0	ER-Golgi trafficking
4p16.1	4	7475 163	rs76278520	C	0.02												**SORCS2**						MFC, ITC	MFC, ITC	N	0	0	ER-Golgi trafficking
4q32.3	4	164 710 808	rs139869159	G	0.03										1	2	MARCH1						ITC		N	0	0	ER-Golgi trafficking
5p13.3	5	32 132 726	rs115506299	A	0.01										1		GOLPH3						ITC		N	1	0	ER-Golgi trafficking
5q21.1	5	100 429 877	rs141829134	T	0.01										4	2	[ST8SIA4]						MFC, ITC		N	0	0	ER-Golgi trafficking
7q22.3	7	105 842 968	rs35447353	G	0.02										1		[NAMPT]						Cer, MFC, ITC		N	2	0	Circadian
															1		[SYPL1]						ITC		N	0	0	ER-Golgi trafficking
7q36.3	7	158 171 807	rs539682094	T	0.01										1		PTPRN2						MFC, ITC	MFC	N	0	0	ER-Golgi trafficking
11p14.1	11	82 680 867	rs10898066	T	0.36										1	1	**RAB30**						ITC		N	0	0	ER-Golgi trafficking

(Continues)

TABLE 3 | (Continued)

Locus						Postmortem brain Fe					Blood Fe				Brain MRI		Candidate gene	Candidate gene selection criteria				Data-driven gene prioritization			Knowledge-driven gene prioritization			
Cytogenetic band	Chromosome	Position (GRCh37/hg19)	dbSNP	Effect allele	Effect allele frequency	ACC	MFC	ITC	Cerebellum	Spleen	S-Iron	TSP	Ferritin	TIBC	8 regions, left & right side (16 total, see Figure 2)[b]	4 regions, left & right side (8 total, see Figure 2 and Methods)[b]	Tier 1, tier 2, [tier 3] candidate genes	Positional (+/− 10 kb)	cis-eQTL (brain, blood)	CI (HiC, Brain)	mQTL (brain)	Brain Fe-RNAseq	Brain Fe-DNA-H3K9ac	Brain Fe-DNA-CpG	Fe/Ferroptosis pathway (direct/seed gene)[c]	STRING (all data types, confidence > 0.7) (indirect)[d]	STRING (experiments confidence > 0.4) (indirect)[d]	Proposed Pathway
11q24.1	11	121 449 806	rs144916412	A	0.01										1		**SORL1**					ACC	MFC, ITC		N	1	0	ER-Golgi trafficking
11q25	11	134 489 534	rs76342262	C	0.02												[B3GAT1]						ITC		N	0	0	ER-Golgi trafficking
15q26.3	15	101 802 184	rs116852966	A	0.04												SELENOS						MFC, ITC	ITC	N	2	0	ER-Golgi trafficking
17q22	17	57 513 988	rs148427669	C	0.03										1	2	CLTC						ITC		Y	12	6	ER-Golgi trafficking
3q27.3	3	186 370 454	rs150042143	T	0.03												FETUB, HRG[e]						MFC, ITC		N	2	0	Heparan Sulfate
4p16.1	4	10 859 478	rs114188639	C	0.03											1	[HS3ST1]						MFC, ITC		N	0	0	Heparan Sulfate
16p12.1	16	25 738 025	rs117940188	G	0.02										2		HS3ST4								N	0	0	Heparan Sulfate
2p23.3	2	27 433 333	rs183148239	T	0.02										3	1	SLC5A6								N	0	0	Coenzyme A
															3	1	SNX17						ITC	MFC	N	0	0	ER-Golgi trafficking
5q34	5	168 035 689	rs111659270	T	0.01										9	1	[PANK3]								N	2	0	Coenzyme A
17q24.1	17	63 392 730	rs72862451	C	0.03										3		[AXIN2]						ITC		N	8	1	Wnt signaling
11p15.2	11	13 148 097	rs150429244	A	0.01										2	1	BMAL1					ACC	Cer, ITC		N	3	2	Circadian
12q24.31	12	121 223 159	rs77431485	A	0.01										1		COQ5						ITC		N	1	0	Coenzyme Q10
17p13.2	17	4 328 402	rs6502784	T	0.08										1		**SPNS3**							ITC	N	0	0	Sphingolipid transport
															1		SLC25A11							MFC, ITC	N	0	0	Mitochondrial transporter

(Continues)

TABLE 3 | (Continued)

Locus						Postmortem brain Fe					Blood Fe				Brain MRI		Candidate gene	Candidate gene selection criteria				Data-driven gene prioritization			Knowledge-driven gene prioritization			
Cytogenetic band	Chromosome	Position (GRCh37/hg19)	dbSNP	Effect allele	Effect allele frequency	ACC	MFC	ITC	Cerebellum	Spleen	S-Iron	TSP	Ferritin	TIBC	8 regions, left & right side (16 total, see Figure 2)[b]	4 regions, left & right side (8 total, see Figure 2 and Methods)[b]	Tier 1, tier 2, [tier 3] candidate genes	Positional (+/− 10 kb)	cis-eQTL (brain, blood)	CI (HiC, Brain)	mQTL (brain)	Brain Fe-RNAseq	Brain Fe-DNA-H3K9ac	Brain Fe-DNA-CpG	Fe/Ferroptosis pathway (direct/seed gene)[c]	STRING (all data types, confidence > 0.7) (indirect)[d]	STRING (experiments confidence > 0.4) (indirect)[d]	Proposed Pathway
															1		RNF167						MFC, ITC	MFC, ITC	N	0	0	ER-Golgi trafficking
															1		SPNS2						MFC, ITC	ITC	N	0	0	Sphingolipid transport
17q23.3	17	61 536 308	rs9896864	G	0.02										1		CYB561						MFC	MFC	Y	1	0	Cellular iron regulation
						$p < 5E\text{-}8 <$		$p < 5E\text{-}6 <$		$p < 0.05$	Direction of effect+												+ associated with PM Fe					
						$p < 5E\text{-}8 <$		$p < 5E\text{-}6 <$		$p < 0.05$	Direction of effect—												− associated with PM Fe					

Note: Genes in bold-face are tier 1 genes; they meet two or more candidate gene selection criteria (columns 19–22). Significance for color shaded values are defined in the bottom two rows.

Abbreviations: ACC, anterior cingulate cortex; Fe, iron; ITC, inferior temporal cortex; MFC, mid frontal cortex; MRI, magnetic resonance imaging; PM, postmortem; QSM, quantitative susceptibility mapping; S-Iron, serum iron; SN, substantia nigra; SNP, single nucleotide polymorphism; TIBC, total iron binding capacity; TSP, transferrin saturation percentage.

♦Index SNP $p < 5E\text{-}8$.

[a]Selected results for novel loci and corresponding prioritized candidate gene inferred by replication, ROSMAP omic results, and biological plausibility. See Table S7 for results of all novel loci meeting criteria.

[b]Number of regions impacted (see Table S7 for details).

[c]Seed gene in pathway: Y, yes; N, no.

[d]Number of seed genes interacting with candidate gene (see Table S7 for details).

[e]V2G candidate.

with higher spleen-Fe and QSM putamen-L/R and hippocampus-R ($p < 0.05$). The nearby candidate *AXIN2* encodes conductin, which organizes a multiprotein complex that initiates ubiquitin-ligase-mediated degradation of β-catenin and, in turn, inhibition of Wnt signaling (Goto et al. 2016). The rs9896864 G variant at 17q23.3 was associated with higher PM ITC Fe and also associated with higher ferritin but lower QSM accumbens-R. Postmortem Fe inversely correlated with H3k9ac and positively correlated with CpG at the mQTL candidate *CYB561*. *CYB561* encodes a trans-membrane di-heme protein notably involved in ascorbate recycling but also functions in ascorbate-mediated trans-membrane Fe3 + −reductase activity (Asard et al. 2013). The rs77431485 A variant at 12q24.31 was associated with higher PM ITC Fe ($p < 5 \times 10^{-6}$) and also associated with higher QSM putamen-R ($p < 0.05$). The eQTL candidate *COQ5* encodes a methyltransferase required for the only C-methylation step in the synthesis of CoQ (ubiquinone), an essential lipophilic electron carrier in the mitochondrial respiratory chain (Nguyen et al. 2014). The rs150429244 A variant at 11p15.2 was associated with higher PM cerebellum Fe ($p < 5 \times 10^{-6}$) and associated with higher QSM SN-L/R and lower T2*SN-R ($p < 0.05$). The eQTL candidate *BMAL1* encodes a transcription factor which, together with CLOCK, drives the circadian clock pathway (Hogenesch et al. 1998). BMAL1 also antagonizes ferroptosis by transcriptionally repressing the expression of *EGLN2* and sequentially activating HIF1A (involved in hypoxia response; Yang et al. 2019). The rs6502784 T variant at 17p13.2 is associated with higher PM MFC Fe ($p < 5 \times 10^{-6}$) and associated with higher QSM hippocampus-R and spans several potential candidates. Among these is *SLC25A11* encoding a mitochondrial carrier protein (Iacobazzi et al. 1992) that also interacts with FUNDC2 to regulate mitochondrial GSH levels and indirectly regulates ferroptosis (Ta et al. 2022). V2G prioritized *ALOX15*, encoding a non-heme Fe-containing dioxygenase that catalyzes the stereo-specific peroxidation of free and esterified polyunsaturated fatty acids (Andersson et al. 2006; Horn et al. 2013; Kuhn et al. 1993; Perry et al. 2020; Sloane et al. 1991; Teder, Boeglin, and Brash 2014). ALOX15 may mediate the translation of oxidative stress to lipid peroxidation and ferroptosis (Singh and Rao 2019).

3.8 | Candidate Gene Selection and Prioritization for Replicated Published Fe Loci

Published Fe loci that were at least nominally associated with PM Fe mapped to 240 candidate genes; 213 of these were expressed in the brain (Table S8). A subset of replicated loci and corresponding prioritized genes (Table 4) are discussed below. Omic measures of most candidate genes spanning replicated loci align with low transcription activity with PM Fe accumulation.

3.8.1 | Cellular Iron Regulation

Variants at 3q29 (*TFRC*), 6p22.2-p21.3 (MHC), and 15q25.1 (*IREB2*) associated with blood Fe and brain MRI-derived Fe traits in GWAS were also nominally associated with PM Fe ($p < 0.05$). *TFRC* encodes the key receptor for cellular Fe uptake (Hentze et al. 2010). The MHC region hosts several independent SNPs associated with Fe and overlaps multiple candidates but most notably *HFE*. *HFE* encodes a homeostatic Fe regulator which binds to receptors TFRC and TFR2; ultimately impacting Fe absorption via both cellular and systemic Fe regulatory pathways (Hentze et al. 2010). *IREB2* encodes an RNA-binding protein that, under low cellular Fe conditions, regulates post-transcriptional expression of several Fe-related genes by binding to Fe-responsive elements (IREs) in the 5′-UTR (inhibiting translation of *FTL/FTH1* (ferritin), *HIF2A/EPAS1, SLC40A1, ACO2*, and *ALAS2*) or 3′-UTR (stabilizing/promoting translation of *TFRC, EGLN3, SLC11A2*, and *HAO1*) of mRNA effectively favoring cellular import of Fe (Sanchez et al. 2011; Hentze et al. 2010). In Fe-replete cells, IREB2 is degraded by FBXL5, promoting storage of Fe in ferritin (Sanchez et al. 2011; Hentze et al. 2010).

Variants at 2q32.2 (*SLC40A1*), 4q24 (*SLC39A8*), and 11q12.3 (*FTH1*) associated with several QSM IDPs in GWAS were nominally associated with PM Fe in the current study as well as select blood Fe traits. *SLC40A1* encodes the only known Fe(2+) exporter ferroportin (Aschemeyer et al. 2018; Hentze et al. 2010). *SLC39A8* encodes a divalent metal ion transporter (ZIP8) that functions in cellular import of zinc, Fe, manganese, and cadmium (Wang et al. 2012). *FTH1* encodes the heavy subunit of ferritin (Treffry et al. 1997; Hentze et al. 2010).

Variants at 4q24 and 7p22.2 GW to nominally associated with several QSM and T2* IDPs also associated with PM Fe but no peripheral Fe traits. *BDH2* and *CISD2* are both potential candidates residing at 4q24. *BDH2* encodes a key enzyme in ketogenesis but also a rate-limiting step in the formation of 2,5-dihydroxybenzoate, a siderophore that delivers/removes Fe3+ from the cell in association with lipocalin-2 (Guo et al. 2006; Liu, Ciocea, and Devireddy 2014). *CISD2* encodes an Fe-S cluster protein found in the outer mitochondrial membrane and ER and has a role in cellular Fe and calcium regulation as well as ferroptosis and autophagy (Wiley et al. 2007; Tamir et al. 2015). *MAFK* resides at 7p22.2 and encodes a transcription factor that, among other functions, suppresses transcription at sites of *NFE2* (Toki et al. 1997), which targets two heme biosynthetic enzymes, hydroxymethylbilane synthase (HMBS) and ferrochelatase (FECH). MAFK also dimerizes with BACH1 to upregulate the expression of *HMOX1*, *FTH1*, *FTL1* (light subunit of ferritin), and *SLC40A1* (Nishizawa et al. 2020).

Index SNP rs28715334 T at 14q11.2 associated with higher ferritin in GWAS was nominally associated with higher PM cerebellum/global Fe. The candidate *SLC7A8* encodes an L-type amino acid transporter that associates with SLC3A2 to form a high-affinity obligatory exchanger for all neutral amino acids (Fotiadis, Kanai, and Palacín 2013). SLC7A8 may function along SLC3A2/SLC7A11 (System X_c) to maintain rate-limiting precursors (i.e., cysteine) for synthesis of GSH (Parker et al. 2021; Fotiadis, Kanai, and Palacín 2013), which is required in redox and Fe homeostasis (Daniel et al. 2020).

TABLE 4 | Subset of published Fe loci replicated in postmortem Fe and prioritized candidate genes[a].

Locus						Postmortem brain						Blood				Brain MRI QSM Fe	Brain MRI T2*	Candidate gene	Candidate gene selection criteria				Data-driven gene prioritization			Knowledge-driven gene prioritization			
Cytogenetic band	Chromosome	Position (GRCh37/hg19)	dbSNP	Effect Allele	Effect Allele Frequency	ACC	MFC	ITC	Cerebellum	spleen	liver[b]	S-Iron	TSP	Ferritin	TIBC	8 regions, left & right side (16 total, see Figure 2)[c]	8 regions, left & right side (16 total, see Figure 2)[c]	Tier 1, Tier 2, [Tier 3] candidate genes	Positional (+/− 10 kb)	cis-eQTL (brain, blood)	CI (HiC, Brain)	mQTL (brain)	Fe-RNAseq	Fe-DNA-H3K9ac	Fe-DNA-CpG	Fe/Ferroptosis pathway (Direct/Seed gene)[d]	STRING (all data types, confidence > 0.7) (indirect)[e]	STRING (experiments confidence > 0.4) (indirect)[e]	Proposed pathway
1p36.12	1	20898514	rs477190	C	0.60									♦				PINK1								N	26	7	Mitochondrial function
10q22.3	10	81073027	rs146292747	Ins[f]	0.78							♦						PPIF						ITC		N	5	1	Mitochondrial function
19p13.3	19	5840619	rs708686	C	0.29									♦		1		**FUT6**					EM			N	0	0	ER-Golgi trafficking
																		FUT3						MFC, ITC	MFC	N	0	0	ER-Golgi trafficking
																		LONP1							MFC	N	3	0	Mitochondrial function
10p12.33	10	17756975	rs45470994	A	0.98											6♦	3♦	STAM						MFC, ITC		N	6	5	ER-Golgi trafficking
																8	3												
19p13.11	19	19436229	rs111234557	G	0.11									♦				BORCS8-MEF2B						MFC, ITC	ACC	N	0	0	ER-Golgi trafficking
																		ATP13A1						MFC		N	0	0	ER-Golgi trafficking/ Mitochondrial function
1q24.2	1	169519049	rs6025	T	0.01								♦	♦	♦	9	1	F5					ACC	ITC		N	0	0	Blood coagulation
8p11.21	8	41630447	rs4737010	G	0.41					♦								**ANK1**						MFC	MFC	Y	5	3	Erythrocyte stability
2q14.2	2	121306440	rs17050272	A	0.45									♦				[INHBB]						ITC		N	1	0	Systemic iron regulation

(Continues)

TABLE 4 | (Continued)

Locus						Postmortem brain						Blood				Brain MRI QSM Fe				Brain MRI T2*			Candidate gene	Candidate gene selection criteria				Data-driven gene prioritization			Knowledge-driven gene prioritization			
Cytogenetic band	Chromosome	Position (GRCh37/hg19)	dbSNP	Effect Allele	Effect Allele Frequency	ACC	MFC	ITC	Cerebellum	spleen	liver[b]	S-Iron	TSP	Ferritin	TIBC	8 regions, left & right side (16 total, see Figure 2)[c]				8 regions, left & right side (16 total, see Figure 2)[c]			Tier 1, Tier 2, [Tier 3] candidate genes	Positional (+/− 10 kb)	cis-eQTL (brain, blood)	CI (HiC, Brain)	mQTL (brain)	Fe-RNAseq	Fe-DNA-H3K9ac	Fe-DNA-CpG	Fe/Ferroptosis pathway (Direct/Seed gene)[d]	STRING (all data types, confidence > 0.7) (indirect)[e]	STRING (experiments confidence > 0.4) (indirect)[e]	Proposed pathway
2q32.2	2	190 377 370	rs10206543	G	0.42											2◆	4	2	3	2	2◆	2	SLC40A1								Y	16	1	Cellular iron regulation
2q32.2	2	190 387 487	rs13008704	C	0.51									◆		3	2	2		1	2		SLC40A1								Y	16	1	Cellular iron regulation
2q32.2	2	190 440 809	rs34206448	T	0.73											4	3	3		2◆	2		**SLC40A1**								Y	16	1	Cellular iron regulation
3q29	3	195 776 976	rs406271	C	0.35											4◆	2			2			**TFRC**						MFC		Y	23	5	Cellular iron regulation
3q29	3	195 814 264	rs111625920	T	0.29											3	3			1◆	2		**TFRC**						MFC		Y	23	5	Cellular iron regulation
3q29	3	195 831 098	rs9867473	A	0.45											4◆	3			2			TFRC						MFC		Y	23	5	Cellular iron regulation
4q24	4	103 146 890	rs35518360	A	0.91											2	6	2		2			SLC39A8						MFC, ITC		Y	4	0	Cellular iron regulation
4q24	4	103 188 709	rs13107325	T	0.08											6◆	2	2◆		6◆	1		**SLC39A8**						MFC, ITC		Y	4	0	Cellular iron regulation
4q24	4	103 685 218	rs28584184	T	0.03											5◆	2	1		2			BDH2						ITC		N	0	0	Cellular iron regulation
																							CISD2							ACC	N	1	0	Cellular iron regulation
6p22.2	6	25 330 116	rs79108775	T	0.08											4◆	6	1		2◆	3		CARMIL1						Cer, MFC, ITC		N	0	0	Actin polymerization

(Continues)

TABLE 4 | (Continued)

Locus						Postmortem brain						Blood				Brain MRI QSM Fe		Brain MRI T2*		Candidate gene	Candidate gene selection criteria				Data-driven gene prioritization		Knowledge-driven gene prioritization			
Cytogenetic band	Chromosome	Position (GRCh37/hg19)	dbSNP	Effect Allele	Effect Allele Frequency	ACC	MFC	ITC	Cerebellum	spleen	liver[b]	S-Iron	TSP	Ferritin	TIBC	8 regions, left & right side (16 total, see Figure 2)[c]		8 regions, left & right side (16 total, see Figure 2)[c]		Tier 1, Tier 2, [Tier 3] candidate genes	Positional (+/− 10 kb)	cis-eQTL (brain, blood)	CI (HiC, Brain)	mQTL (brain)	Fe-RNAseq	Fe-DNA-H3K9ac	Fe-DNA-CpG	Fe/Ferroptosis pathway (Direct/Seed gene)[d]	STRING (all data types, confidence > 0.7) (indirect)[e]	STRING (experiments confidence > 0.4) (indirect)[e]	Proposed pathway
6p22.2	6	25 348 616	rs139436607	C	0.10											4	8	3		HIST1H2BD						MFC, ITC		N	4	0	Nucleosome/ DNA accessibility
6p22.2	6	25 392 326	rs192533405	A	0.07											4	7	1	3	CARMIL1						Cer, MFC, ITC		N	0	0	Actin polymerization
6p22.2	6	25 526 319	rs149359690	T	0.07											6	7	1	3	**CARMIL1**						Cer, MFC, ITC		N	0	0	Actin polymerization
																				HIST1H4H						ITC		Y	9	15	Nucleosome/ DNA accessibility
6p22.2	6	26 072 992	rs144861591	T	0.04											9	5	2	4	HIST1H4H						ITC		Y	9	15	Nucleosome/ DNA accessibility
																				HIST1H2BD						MFC, ITC		N	4	0	Nucleosome/ DNA accessibility
																				HIST1H1C						ACC, MFC		N	3	2	Nucleosome/ DNA accessibility
6p22.2	6	26 093 141	rs1800562	A	0.04											9	4	8	4	HFE						ITC		N	12	5	Cellular/ Systemic iron regulation

(Continues)

TABLE 4 | (Continued)

Locus						Postmortem brain						Blood				Brain MRI QSM Fe		Brain MRI T2*		Candidate gene	Candidate gene selection criteria				Data-driven gene prioritization			Knowledge-driven gene prioritization			
Cytogenetic band	Chromosome	Position (GRCh37/hg19)	dbSNP	Effect Allele	Effect Allele Frequency	ACC	MFC	ITC	Cerebellum	spleen	liver[b]	S-Iron	TSP	Ferritin	TIBC	8 regions, left & right side (16 total, see Figure 2)[c]		8 regions, left & right side (16 total, see Figure 2)[c]		Tier 1, Tier 2, [Tier 3] candidate genes	Positional (+/− 10 kb)	cis-eQTL (brain, blood)	CI (HiC, Brain)	mQTL (brain)	Fe-RNAseq	Fe-DNA-H3K9ac	Fe-DNA-CpG	Fe/Ferroptosis pathway (Direct/Seed gene)[d]	STRING (all data types, confidence > 0.7) (indirect)[e]	STRING (experiments confidence > 0.4) (indirect)[e]	Proposed pathway
6p22.2	6	26098474	rs79220007	C	0.04											9	5	2	4	HFE						ITC		Y	12	5	Cellular/ Systemic iron regulation
6p22.2	6	26123502	rs115740542	C	0.04											9	5	2	4	HIST1H2BC								N	5	5	Nucleosome/ DNA accessibility
6p22.1	6	27122444	rs71559014	G	0.07											4	8	1	5	**ZNF322**						MFC, ITC		N	0	0	Transcription factor
																				HIST1H2BK							ACC	N	4	3	Nucleosome/ DNA accessibility
																				HIST1H2BO						ACC, Cer, ITC	ACC	N	5	1	Nucleosome/ DNA accessibility
																				HMGN4						ITC		N	0	0	Nucleosome/ gene transcription
																				HIST1H2AK						MFC, ITC	ACC	N	1	1	Nucleosome/ DNA accessibility
6p22.1	6	27209978	rs34446632	T	0.07											4	9			PRSS16						MFC, ITC	ACC	N	0	0	Serine protease/ Thymus

(Continues)

TABLE 4 | (Continued)

Locus						Postmortem brain						Blood				Brain MRI QSM Fe	Brain MRI T2*	Candidate gene	Candidate gene selection criteria				Data-driven gene prioritization			Knowledge-driven gene prioritization			
Cytogenetic band	Chromosome	Position (GRCh37/hg19)	dbSNP	Effect Allele	Effect Allele Frequency	ACC	MFC	ITC	Cerebellum	spleen	liver[b]	S-Iron	TSP	Ferritin	TIBC	8 regions, left & right side (16 total, see Figure 2)[c]	8 regions, left & right side (16 total, see Figure 2)[c]	Tier 1, Tier 2, [Tier 3] candidate genes	Positional (+/− 10kb)	cis-eQTL (brain, blood)	CI (HiC, Brain)	mQTL (brain)	Fe-RNAseq	Fe-DNA-H3K9ac	Fe-DNA-CpG	Fe/Ferroptosis pathway (Direct/Seed gene)[d]	STRING (all data types, confidence > 0.7) (indirect)[e]	STRING (experiments confidence > 0.4) (indirect)[e]	Proposed pathway
6p22.1	6	27224588	rs61740410	A	0.07											4♦	1♦	HIST1H4H						ITC		Y	9	15	Nucleosome/ DNA accessibility
6p22.1	6	27497148	rs6908155	A	0.25						♦					6	1	ZSCAN9					ACC, ITC	ITC		N	0	0	DNA binding
6p21.33	6	31333032	rs9266366	T	0.11											1♦ 9	2	**TCF19**							MFC, ITC	N	1	0	Transcription factor
																		HLA-C							MFC	N	4	2	Antigen-presenting MHC molecule
																		HLA-B						Cer, MFC, ITC		N	4	2	Antigen-presenting MHC molecule
																		VARS2						MFC, ITC	MFC	N	1	0	Mitochondrial tRNA aminoacylation
																		POU5F1					Cer	ITC	MFC, ITC	N	8	0	Transcription factor
																		PSORS1C1					Cer		MFC, ITC	N	0	0	Psoriasis Susceptibility
																		AIF1						ITC	MFC	N	1	0	Actin/calcium binding

(Continues)

TABLE 4 | (Continued)

Locus						Postmortem brain					Blood				Brain MRI QSM Fe		Brain MRI T2*		Candidate gene	Candidate gene selection criteria				Data-driven gene prioritization			Knowledge-driven gene prioritization			
Cytogenetic band	Chromosome	Position (GRCh37/hg19)	dbSNP	Effect Allele	Effect Allele Frequency	ACC	MFC	ITC	Cerebellum	spleen	liver[b]	S-Iron	TSP	Ferritin	TIBC	8 regions, left & right side (16 total, see Figure 2)[c]		8 regions, left & right side (16 total, see Figure 2)[c]		Tier 1, Tier 2, [Tier 3] candidate genes	Positional (+/− 10 kb)	cis-eQTL (brain, blood)	CI (HiC, Brain)	mQTL (brain)	Fe-RNAseq	Fe-DNA-H3K9ac	Fe-DNA-CpG	Fe/Ferroptosis pathway (Direct/Seed gene)[d]	STRING (all data types, confidence > 0.7) (indirect)[e]	STRING (experiments confidence > 0.4) (indirect)[e]	Proposed pathway
6p21.32	6	32 389 255	rs3135365	C	0.19											2♦	5	2		HLA-DQB1					Cer			Y	4	1	Antigen-presenting MHC molecule
																				HLA-DRB5							ACC	N	5	0	Antigen-presenting MHC molecule
																				C2						ITC	MFC	N	2	0	Complement cascade
																				LTA						MFC	MFC	N	1	0	TNF cytokine
																				PSMB9						ITC	MFC	N	8	2	Proteasome subunit
																				NOTCH4						MFC, ITC	MFC, ITC	N	9	0	Cell–cell signaling
7p22.2	7	1 575 089	rs61423551	A	0.58											4♦	11	1♦	3	**MAFK**					MFC		MFC, ITC	N	5	3	Cellular iron regulation
11q12.3	11	61 765 133	rs10736716	G	0.64											9♦	5	3♦	6	**FTH1**						ITC		Y	9	3	Cellular iron regulation

(Continues)

TABLE 4 | (Continued)

Locus						Postmortem brain						Blood				Brain MRI QSM Fe		Brain MRI T2*		Candidate gene	Candidate gene selection criteria				Data-driven gene prioritization			Knowledge-driven gene prioritization			
Cytogenetic band	Chromosome	Position (GRCh37/hg19)	dbSNP	Effect Allele	Effect Allele Frequency	ACC	MFC	ITC	Cerebellum	spleen	liver[b]	S-Iron	TSP	Ferritin	TIBC	8 regions, left & right side (16 total, see Figure 2)[c]		8 regions, left & right side (16 total, see Figure 2)[c]		Tier 1, Tier 2, [Tier 3] candidate genes	Positional (+/− 10kb)	cis-eQTL (brain, blood)	CI (HiC, Brain)	mQTL (brain)	Fe-RNAseq	Fe-DNA-H3K9ac	Fe-DNA-CpG	Fe/Ferroptosis pathway (Direct/Seed gene)[d]	STRING (all data types, confidence > 0.7) (indirect)[e]	STRING (experiments confidence > 0.4) (indirect)[e]	Proposed pathway
14q11.2	14	23 635 213	rs28715334	T	0.18									♦						**SLC7A8**					MFC	MFC, ITC		N	2	1	Cellular iron regulation
15q25.1	15	78 771 186	rs11634990	T	0.18									♦		2	1	2		**IREB2**								Y	18	4	Cellular iron regulation
19q13.12	19	35 950 523	rs12975762	A	0.29							♦						1		TMEM147, HAMP[g]							ACC	N	0	0	Systemic iron regulation
22q12.3	22	37 462 936	rs855791	G	0.61						♦	♦	♦		♦	4	8	♦1	2	TMPRSS6					EM			Y	8	1	Systemic iron regulation
22q12.3	22	37 469 192	rs6000553	G	0.58											4♦	8	♦2	2	TMPRSS6					EM			Y	8	1	Systemic iron regulation

(Continues)

TABLE 4 | (Continued)

Locus						Postmortem brain						Blood				Brain MRI QSM Fe	Brain MRI T2*	Candidate gene	Candidate gene selection criteria				Data-driven gene prioritization			Knowledge-driven gene prioritization			
Cytogenetic band	Chromosome	Position (GRCh37/hg19)	dbSNP	Effect Allele	Effect Allele Frequency	ACC	MFC	ITC	Cerebellum	spleen	liver[b]	S-Iron	TSP	Ferritin	TIBC	8 regions, left & right side (16 total, see Figure 2)[c]	8 regions, left & right side (16 total, see Figure 2)[c]	Tier 1, Tier 2, [Tier 3] candidate genes	Positional (+/− 10 kb)	cis-eQTL (brain, blood)	CI (HiC, Brain)	mQTL (brain)	Fe-RNAseq	Fe-DNA-H3K9ac	Fe-DNA-CpG	Fe/Ferroptosis pathway (Direct/Seed gene)[d]	STRING (all data types, confidence > 0.7) (indirect)[e]	STRING (experiments confidence > 0.4) (indirect)[e]	Proposed pathway
22q12.3	22	37470041	rs2076085	A	0.58							♦				4	8		2		**TMPRSS6**			EM			Y	8	1	Systemic iron regulation
						$p<5E\text{-}8<$		$p<5E\text{-}6<$		$p<0.05$		Direction of effect+													+ associated with PM Fe					
						$p<5E\text{-}8<$		$p<5E\text{-}6<$		$p<0.05$		Direction of effect—													- associated with PM Fe					

Note: Genes in bold-face are tier 1 genes; they meet two or more candidate gene selection criteria (columns 19-22). Significance is defined in the bottom two rows.
Abbreviations: ACC, anterior cingulate cortex; EM, excess missing; Fe, iron; ITC, inferior temporal cortex; MFC, mid frontal cortex; MRI, magnetic resonance imaging; PM, postmortem; QSM, quantitative susceptibility mapping; S-Iron, serum iron; SN, substantia nigra; SNP, single nucleotide polymorphism; TIBC, total iron binding capacity; TSP, transferrin saturation percentage.

♦Index SNP $p<5E\text{-}8$.

[a]Selected results for published Fe loci replicated in postmortem Fe ($p<0.05$) and prioritized candidate gene inferred by ROSMAP omic results and biological plausibility. See Table S8 for all replicated loci ($p<0.05$).

[b]Direction of effect not reported.

[c]Number of regions impacted (see Table S8 for details).

[d]Seed gene in pathway: Y, yes; N, no.

[e]Number of seed genes interacting with candidate gene (see Table S8 for details).

[f]Ins, insertion: CCCACCCACCA.

[g]V2G candidate.

3.8.2 | Systemic Iron Regulation

Variants at 2q14.2 (*INHBB*), 19q13.12 (*HAMP*), and 22q12.3 (*TMPRSS6*), previously associated with several Fe traits in GWAS, were also nominally associated with PM ACC Fe. *HAMP* (prioritized by V2G) encodes hepcidin (Hentze et al. 2010). *INHBB* encodes inhibin-βB that is reportedly induced in response to inflammation which, in turn, induces activin B and enhances *HAMP* expression (Kanamori et al. 2016). *TMPRSS6* encodes a membrane-bound protease that negatively regulates the expression of *HAMP* (Wang, Meynard, and Lin 2014).

3.8.3 | Mitochondrial Function

Index variants at 1p36.12 (*PINK1*), 10q22.3 (*PPIF*), and 19p13.3 (*LONP1*) associated with higher blood ferritin and Fe in GWAS associated with higher PM MFC and ITC Fe ($p < 0.05$). PINK1 encodes a mitochondrial kinase that phosphorylates proteins such as Parkin (*PRKN*) to coordinate the removal or replacement of dysfunctional mitochondrial components (mitophagy; Kane et al. 2014). *PINK1* and *PRKN* mutations are associated with young-onset PD (Muñoz et al. 2016). In cancer models, loss of *PINK1* promotes Fe accumulation in serum and mitochondria; the latter mediated by increased expression of mitoferrin-1 (*SLC25A37*) and mitoferrin −2 (*SLC25A28*; Kang et al. 2019). *PPIF* encodes a member of the mitochondrial permeability transition pore (Elrod and Molkentin 2013). *LONP1* encodes a multifunctional mitochondrial enzyme (Gibellini et al. 2020). As a protease it selectively degrades misfolded or oxidized proteins such as 5-aminolevulinate synthase (ALAS1), mitochondrial aconitase (ACO2), Cystathionine β-synthase (CBS), DELE1, and PINK1, all implicated in Fe homeostatic or responsive pathways (Lu et al. 2007; Gibellini et al. 2020; Bota and Davies 2002; Teng et al. 2013; Zhou et al. 2018; Sekine et al. 2023).

3.8.4 | Others

Published variants mapping to candidates with potential roles in blood coagulation (1q24.2, *F5*), erythrocyte membrane stability (8p11.21, *ANK1*), and ER-Golgi trafficking (*BORCS8*, *ATP13A1*) were also replicated in PM brain Fe (Vallese et al. 2022; Pu et al. 2015; McKenna et al. 2020).

4 | Discussion

In this first GWAS of PM Fe we implemented a multistep integrative strategy to identify loci which leverages paired molecular data, prior knowledge, and published GWAS results. With the exceptions of *CLTC*, *MARCH1*, *HRG*, and *CYB561*, most potentially novel loci identified for PM Fe had no direct links to Fe regulatory pathways. However, replication of a subset of prior loci for blood Fe suggests that genetic determinants or biological pathways underlying Fe accumulation in the brain are not completely distinct from those of Fe circulating in the periphery. For several novel and replicated published loci the direction of effects was not aligned and this might be explained by the differential distribution or function of Fe across and within tissue. When DLPFC omic markers of candidate genes converged with PM Fe accumulation they most often impacted MFC and ITC and aligned with lower transcription activity.

Iron metabolism is generally balanced by two regulatory pathways. The first functions systemically, relies on hepcidin and ferroportin, and is regulated by Fe-status (via BMP/SMAD signaling) and inflammation (via IL6/JAK/STAT3 signaling; Hentze et al. 2010). The second controls cellular Fe metabolism by a post-transcriptional mechanism mediated by iron-regulatory proteins (IRP1 and IRP2) and is indirectly regulated by cellular Fe levels, oxygen levels, and the activity of the Fe–S cluster biosynthetic pathway (Galy, Conrad, and Muckenthaler 2024; Hentze et al. 2010). These pathways are thought to be generally shared across organs (Ke and Qian 2007). Indeed, replication in PM Fe of some previously published loci in both Fe regulatory pathways would partly support this argument. Other loci were not replicated, but given a subset was associated with both blood Fe traits and brain MRI-derived measures (Table S8), we cannot rule out the possibility that these are also generalizable loci for Fe. For example, variants at 3q22.1 (*TF*), 4p15.32 (*FBXL5*), 7q22.1 (*TFR2*), and 8p21.2 (*SLC25A37*) associate with both blood and brain MRI-derived Fe traits and all map to candidate genes linked to cellular iron metabolism (Hentze et al. 2010). IL6, the ligand for the receptor encoded by *IL6R* (1q21.3), positively regulates hepcidin expression during systemic inflammation (Hentze et al. 2010). Genes encoding known or putative Fe transporters map to variants at 12q13.12 (*SLC11A2/DMT1*), 11p11.2 (*SLC39A13/ZIP13*), 10p12.33 (*SLC39A12*), and 4q22.1 (*ABCG2*; Hentze et al. 2010; Xu, Wan, and Zhou 2019; Desuzinges-Mandon et al. 2010). Variants at 1q42.2 (*EGLN1*) and 14q13.1 (*EGLN3*) mapping to genes encoding oxygen-dependent hypoxia-inducible factor (HIF) hydroxylating dioxygenases (Ivan and Kaelin 2017) also replicated across blood and brain MRI-derived Fe traits.

Genetic variation underlying a response mechanism that uniquely summons Fe for utilization but protects the brain from excess Fe or its consequences (i.e., ferroptosis) may be of high priority to the brain. For this reason, we applied a hybrid approach to discovery rather than exclusive reliance on replication. We provide support for novel loci linked to pathways that may have greater relevance to brain Fe accumulation including ER-Golgi trafficking, HS, and CoA. Our results also lend support to the role of circadian rhythms and mitochondria function in Fe regulation more generally. ER-Golgi trafficking functions in the delivery of proteins newly synthesized in the ER to their final destinations and in the internalization of proteins for recycling or degradative regulation. The ER and GA house nearly all members of the cellular Fe metabolism and ferroptosis pathways (Long et al. 2022). However, only two of our candidate genes in this pathway have direct links to Fe: *CLTC* (facilitates endocytosis of holo-Tf/TFRC; Royle, Bright, and Lagnado 2005; Tortorella and Karagiannis 2014; McCarthy and Kosman 2012) and *MARCH1* (facilitates endocytosis and sorting to lysosomes of TFRC; Martin et al. 2022). Some novel candidates potentially function in the post-translational modification (PTM) of Tf (*B3GAT1*; Landini et al. 2022) and lactoferrin (*ST8S1A4*; Kühnle et al. 2019). Lactoferrin binds Fe with higher affinity than Tf (Masson, Heremans, and Schonne 1969). The levels of lactoferrin are markedly increased in the brains of AD patients but its origin remains largely unknown (Li and Guo 2021). The novel brain Fe candidate *SORL1* retains APP in

the TGN, preventing its transit through late endosomes where Aβ40 and Aβ42 are generated (Caglayan et al. 2014; Andersen et al. 2005; Nielsen et al. 2007; Fjorback and Andersen 2012). SORL1 may also sort the latter peptides to lysosomes for catabolism (Caglayan et al. 2014). Rare mutations in *SORL1* (i) reduce the capacity of the protein to bind APP, resulting in increased levels of soluble (s) APP (Vardarajan et al. 2015) and (ii) strongly associate with LOAD and EOAD (Barthelson, Newman, and Lardelli 2020). Loss of wild-type sorl1 results in dysregulation of genes with a 3′-UTR IRE, and of genes involved in the cellular response to hypoxia (Barthelson et al. 2020). Neurotoxicity of Aβ is enhanced by Fe. Conversely, α-secretase cleavage of APP releases sAPPα which is potentially neuroprotective and may also modulate Fe efflux by stabilizing ferroportin (McCarthy, Park, and Kosman 2014; Bandyopadhyay and Rogers 2014). SORL1 might therefore indirectly impact Fe homeostasis and toxicity via APP (Barthelson, Newman, and Lardelli 2020). A more common variant in *SORL1* associates with AD in GWAS (Bellenguez et al. 2022) but did not associate with PM Fe in the current study. We previously reported that brain DNA methylation (CpG) of *SORL1* was associated with greater odds of pathological AD diagnosis in ROSMAP (Yu et al. 2015). PM Fe correlated with *SORL1* H3K9ac and RNAseq (also inferring lower transcriptional activity) but did not correlate with *SORL1* CpG. *SORCS2* is another novel candidate and member of the VPS10-related sortilin family but has not been implicated in Fe regulation or neurodegenerative disease. GOLPH3 knockdown of cancer cells present with decreased expression of Fe or ferroptosis-related genes (*SLC7A11, PRNP, MAP 1LC3B, GCLC, SLC39A14, SLC11A2, ATG5, GCLM*, and *SLC40A1*) and promote Erastin-induced ferroptosis (Chen et al. 2024; Yin et al. 2024). GOLPH3 expression positively correlated with *SLC7A11, GPX4*, and *FTH1* expression in cancer models (Yin et al. 2024; Chen et al. 2024). GWAS of Fe-implicated neurodegenerative diseases support additional candidates mapping to the ER-Golgi trafficking pathway such as *ARRDC4* (AD), *SNX1* (AD), *SCARB2* (AD, PD), *MARCH1* (MS), and *TMEM106B* (AD; Lambert et al. 2023; Kim et al. 2024; 2019; Tables S3 and S4). Interplay between Fe and other candidates mapping to ER-Golgi trafficking on neurodegeneration warrants further study.

Independent novel loci for PM Fe map to two HS3ST members that generate 3-O-sulfated glucosaminyl HS with potential roles in hepcidin regulation. HS and heparin are classically known for their anticoagulant actions (Beurskens et al. 2020). Several candidate genes (i.e., *F5*, *TFP1, FN1*, and *SERPINA1*) for variants associated with both blood and brain-derived Fe traits share a role in blood coagulation and thus we cannot discount a role of this pathway connecting *HS3ST*s to PM Fe. Nevertheless, specificity of these loci to brain Fe traits is noteworthy. HSPGs have been implicated in the development and progression of AD (Snow, Cummings, and Lake 2021; Sepulveda-Diaz et al. 2015; Oh et al. 2023; Ferreira et al. 2022; Wang et al. 2023; Jansen et al. 2019; Bellenguez et al. 2022). *HS3ST4* expression is elevated in brains of AD patients (Sepulveda-Diaz et al. 2015). Plasma HS3ST4 levels decrease with (chronological) age, positively correlate with brain age-gap (brain-age—chronological age), and have been used to predict cognitive decline and AD (Oh et al. 2023). HS3ST1-synthesized 3-O-sulfated HS has a role in the binding/uptake of aggregated tau protein and levels are also elevated in the brains of AD patients (Ferreira et al. 2022; Wang et al. 2023). Finally, *HS3ST1*, *HS3ST5*, and *IDUA* (encoding alpha-l-iduronidase required for the lysosomal degradation of HS) are AD risk loci (Jansen et al. 2019; Bellenguez et al. 2022).

Two novel loci mapped to candidates involved in the transport (*SLC5A6*) and phosphorylation (*PANK3*) of pantothenate are essential steps for CoA biosynthesis. *PANK2* (a paralog of *PANK3*) and *COASY* (encoding CoA synthase) are known NBIA genes but, unlike PANK3 and SLC5A6, localize to mitochondria (Di Meo, Carecchio, and Tiranti 2019). Common variants near *COASY* were associated with QSM putamen and caudate in GWAS (Wang et al. 2022) but did not replicate in PM Fe. CoA is essential for fatty acid synthesis and β-oxidation (Mignani et al. 2021). CoA also functions in PTM by the transfer of acyl groups. CoA is the source for the 4′-phosphopantetheine moiety required for the 4′-phosphopantetheinylation needed to activate mitochondrial acyl carrier protein, an essential component of mitochondrial complexes involved in the electron transfer chain, Fe-S cluster assembly, and lipoic acid metabolism. As succinyl-CoA, it contributes to the biosynthesis of hemes, which begins in the mitochondrial matrix with the decarboxylative condensation of glycine with succinyl-CoA to form 5-aminolevulinic acid (ALA), catalyzed by ALAS2 (Layer et al. 2010; Mignani et al. 2021). Why dysfunctions in CoA synthesis lead to Fe accumulation is unclear. Recent work using human iPSC-derived astrocytes suggests it might interfere with endocytic vesicular trafficking, leading to an aberrant Tf receptor-mediated Fe uptake (Ripamonti et al. 2022; Levi et al. 2024). Acetyl-CoA is the sole donor of acetyl groups for palmitoyl transferases. In fibroblasts from patients with Friedreich ataxia (a degenerative disease also presenting with Fe accumulation) and different NBIA sub-types, an impairment in TfR1 palmitoylation results in defective Tf trafficking and TfR1 recycling, leading to intracellular Fe accumulation (Petit et al. 2021; Drecourt et al. 2018). Supplementing cells with CoA increases TfR1 palmitoylation and reduces Fe accumulation. A predominance of mitochondrial gene candidates for brain measures of Fe (Tables 3 and 4) also aligns with a key role of Fe in ATP production and the high-intensity energy metabolism of the brain. *COQ5* (Table 3) encodes a methyltransferase required for the synthesis of CoQ, which may function with ferroptosis suppressor protein 1 (encoded by *AIFM2*) to suppress ferroptosis; independent of glutathione (Bersuker et al. 2019). A recent genome-wide CRISPR interference screen in human neurons reported that the knockdown of COQ5 (and other genes in Fe pathways) was toxic and led to increased Fe levels (Tian et al. 2021). Interestingly, *COQ5* was also an eQTL candidate for an independent variant at 12q24.31 not replicated with PM brain Fe but generalized to blood and brain-MRI Fe traits (Table S8). Mitochondrial dysfunction constitutes one of the hallmarks of aging and neurodegeneration and this is often attributed to Ca2+ dyshomeostasis (Levi et al. 2024). However, the disruption of Fe homeostasis can interfere with mitochondrial functions and, consequently, fuel the progression of neurodegeneration (Ficiarà et al. 2024). Conversely, the alteration of mitochondrial functions may affect mitochondrial Fe homeostasis, leading to Fe accumulation and neurodegeneration (Levi et al. 2024; Muñoz et al. 2016). The latter scenario is supported by our genetic results and is also proposed in PANK-associated neurodegeneration.

A novel candidate for PM Fe that replicated in QSM data was the established circadian gene *BMAL1*. The *CLOCK* locus, while not replicated in PM Fe but generalized to blood and brain MRI traits (Table S8), encodes another key regulator of circadian rhythms that forms a heterodimer with BMAL1. *THRAP3*, a novel candidate for PM Fe, coactivates CLOCK-BMAL1. Serum Fe exhibits diurnal variation that aligns with *Tfrc* oscillations (Ridefelt et al. 2010); the latter ablated in *Bmal1* knockout mice (Weger et al. 2021). Neurodegenerative disorders with reported alterations in brain Fe homeostasis often present with symptoms of altered circadian homeostasis (Nassan and Videnovic 2022). PD patients present with impaired blood cell *BMAL1* expression that correlates with motor severity and sleep quality (Cai et al. 2010; Breen et al. 2014). Cycles of *BMAL1* methylation contribute to the regulation of BMAL1 rhythms in the brain and these rhythms are altered in AD patients (Cronin et al. 2017). *BMAL1* expression in PM frontal cortex correlates with tau pathology, cognitive disturbance, and overnight wakefulness (Hulme et al. 2020). Common variants mapping to other members of the circadian pathway such as *RORA, ADCY3, CAMK2G, GNG2*, and *NR1D1* also associated with PD and MS in GWAS (International Multiple Sclerosis Genetics Consortium 2019; Kim et al. 2024).

Whether Fe contributes to neurodegeneration or elevates as a consequence of the neurodegenerative process is unclear. Accelerated disease progression observed in PD and AD patients taking Fe chelation therapy suggests that Fe has a net positive impact on the brain (Devos et al. 2022; Ayton et al. 2025). Most of our novel PM-Fe loci have links to neurodegeneration but we replicate several others with direct links to Fe pathways thus supporting either argument. Common SNPs associated with neurodegeneration in GWAS and nominally associated with PM Fe (Tables S3–S5) map to very few genes directly related to Fe. One PD risk loci that is nominally associated with PM ITC measures of Fe mapped to *SNCA*, encoding α-synuclein. IREs are located in 5′UTR of *SNCA* (as well as *APP*) mRNA and are proposed therapeutic targets (Rogers and Cahill 2020). Other candidate genes mapping to established AD and PD loci with direct links to Fe yet not associated with PM Fe include *PICALM* (AD), encoding a clathrin assembly protein with a critical role in TfR internalization (Ando et al. 2022), and *ALAS1* (PD), encoding a mitochondrial enzyme for the rate-limiting step in heme biosynthesis (Yien and Perfetto 2022).

Availability of PM brain Fe, genetic data, and other PM brain omic measures from the same individuals are key strengths of the current study. These strengths, however, are limited by the sample size and lack of matching samples for replication. MAP participants with PM brain Fe were old and many presented with AD neuropathology and stroke at the time of death which might confound our GWAS of PM brain Fe or explain loci heterogeneity across brain regions. Models adjusted for dementia and stroke impacted four replicated loci (Table S7) but these loci were not subsequently supported by omic results or biological plausibility. Moreover, loci previously associated with amyloid, tau, stroke infarcts, or brain microbleeds in GWAS were not among our loci taken forward for replication. Some of our novel Fe candidates, despite replication with other Fe traits in younger cohorts, have strong links to neurodegeneration and thus further emphasize the complex relationship between this essential nutrient and brain health. Another limitation is the different brain regions sourcing the Fe and omic measures. Regulation of expression of many proteins involved in Fe metabolism occurs post-translationally and thus caution is warranted when interpreting the omic results. The UKB brain MRI-derived IDPs capture only subcortical tissue while our PM brain Fe and omic measures capture cortical tissue (gray matter). Several loci that appeared specific to Brain-MRI Fe (not replicated in PM brain Fe) may be a function of the larger sample size of UKB or the QSM technique. For example, QSM-specific loci map to *COASY* (17q21.2), *ACO1* (9p21.1), and *HMBS* (11q23.3) and have plausible links to Fe while other significant loci map to genes linked to glia and myelin, extracellular matrix, and calcium homeostasis; pathways also known to affect tissue constituents (Liu et al. 2015). While finalizing our work for submission, Casanova et al. (2024) published a re-analysis of the UKB data and additionally identified loci mapping to *CYBRD1* (2q31.1), *CP* (3q25.1), *SLC39A14* (8p21.3), and *SLC30A10* (1q41) with plausible roles in cellular Fe regulation. They also identified the AD locus 11q14.2 mapping to *PICALM*.

There is increasing interest in using genetic risk scores to evaluate the causal role of Fe in disease spanning several physiological pathways or to identify individuals predisposed to Fe deficiency or toxicity. Leveraging shared genetic effects across Fe-traits may (i) improve score performance for phenome-wide analysis (Kelemen et al. 2024) and (ii) guide the selection of candidate genes for functional characterization. Alternatively, tissue-specific genetic effects may be used to (i) refine scores to facilitate interpretation and (ii) design functional studies. Our genetic findings in the context of other Fe-trait GWAS provide new insight into brain Fe homeostasis.

Author Contributions

Marilyn C. Cornelis: conceptualization, methodology, funding acquisition, writing – original draft, investigation, visualization, writing – review and editing, formal analysis, project administration, data curation. **Amir Fazlollahi:** writing – review and editing, visualization. **David A. Bennett:** funding acquisition, resources, writing – review and editing. **Julie A. Schneider:** funding acquisition, writing – review and editing, resources. **Scott Ayton:** funding acquisition, supervision, resources, data curation, writing – review and editing.

Acknowledgments

Supported by the National Institute on Aging (R01AG065398, R01AG17917, U01AG46152, U01AG61356, R01AG054057). Any opinions, findings, conclusions, or recommendations expressed in this publication are those of the authors and do not necessarily reflect the view of the NIA. We thank the study staff and participants of MAP for their contributions and donations of their brains to these projects. Computations in this paper were run on the Quest cluster supported in part through the computational resources and staff contributions provided for the Quest high-performance computing facility at Northwestern University, which is jointly supported by the Office of the Provost, the Office for Research, and Northwestern University Information Technology.

Conflicts of Interest

The authors declare no conflicts of interest.

Data Availability Statement

The data that support the findings of this study can be requested at www.radc.rush.edu. Summary statistics for the postmortem Fe GWAS are available for download at https://prism.northwestern.edu/.

References

Ackermann, K., S. Khazaipoul, J. L. Wort, et al. 2023. "Investigating Native Metal Ion Binding Sites in Mammalian Histidine-Rich Glycoprotein." *Journal of the American Chemical Society* 145: 8064–8072.

Andersen, O. M., J. Reiche, V. Schmidt, et al. 2005. "Neuronal Sorting Protein-Related Receptor sorLA/LR11 Regulates Processing of the Amyloid Precursor Protein." *Proceedings of the National Academy of Sciences of the United States of America* 102: 13461–13466.

Andersson, E., F. Schain, M. Svedling, H. E. Claesson, and P. K. Forsell. 2006. "Interaction of Human 15-Lipoxygenase-1 With Phosphatidylinositol Bisphosphates Results in Increased Enzyme Activity." *Biochimica et Biophysica Acta* 1761: 1498–1505.

Ando, K., S. Nagaraj, F. Küçükali, et al. 2022. "PICALM and Alzheimer's Disease: An Update and Perspectives." *Cells* 11: 3994.

Angata, K., M. Suzuki, J. McAuliffe, Y. Ding, O. Hindsgaul, and M. Fukuda. 2000. "Differential Biosynthesis of Polysialic Acid on Neural Cell Adhesion Molecule (NCAM) and Oligosaccharide Acceptors by Three Distinct α2, 8-Sialyltransferases, ST8Sia IV (PST), ST8Sia II (STX), and ST8Sia III." *Journal of Biological Chemistry* 275: 18594–18601.

Asard, H., R. Barbaro, P. Trost, and A. Bérczi. 2013. "Cytochromes b 561: Ascorbate-Mediated Trans-Membrane Electron Transport." *Antioxidants & Redox Signaling* 19: 1026–1035.

Aschemeyer, S., B. Qiao, D. Stefanova, et al. 2018. "Structure-Function Analysis of Ferroportin Defines the Binding Site and an Alternative Mechanism of Action of Hepcidin." *Blood* 131: 899–910.

Asperti, M., A. Denardo, M. Gryzik, P. Arosio, and M. Poli. 2019. "The Role of Heparin, Heparanase and Heparan Sulfates in Hepcidin Regulation." *Vitamins and Hormones* 110: 157–188.

Ayton, S., D. Barton, B. Brew, et al. 2025. "Deferiprone in Alzheimer's Disease: A Randomized Clinical Trial." *JAMA Neurology* 82, no. 1: 11–18. https://doi.org/10.1001/jamaneurol.2024.3733.

Ayton, S., N. G. Faux, A. I. Bush, and Alzheimer's Disease Neuroimaging I. 2015. "Ferritin Levels in the Cerebrospinal Fluid Predict Alzheimer's Disease Outcomes and Are Regulated by APOE." *Nature Communications* 6: 6760.

Ayton, S., A. Fazlollahi, P. Bourgeat, et al. 2017. "Cerebral Quantitative Susceptibility Mapping Predicts Amyloid-Beta-Related Cognitive Decline." *Brain* 140: 2112–2119.

Ayton, S., S. Portbury, P. Kalinowski, et al. 2021. "Regional Brain Iron Associated With Deterioration in Alzheimer's Disease: A Large Cohort Study and Theoretical Significance." *Alzheimer's and Dementia* 17, no. 7: 1244–1256. https://doi.org/10.1002/alz.12282.

Bandyopadhyay, S., and J. T. Rogers. 2014. "Alzheimer's Disease Therapeutics Targeted to the Control of Amyloid Precursor Protein Translation: Maintenance of Brain Iron Homeostasis." *Biochemical Pharmacology* 88: 486–494.

Barthelson, K., M. Newman, and M. Lardelli. 2020. "Sorting out the Role of the Sortilin-Related Receptor 1 in Alzheimer's Disease." *Journal of Alzheimer's Disease Reports* 4: 123–140.

Barthelson, K., S. M. Pederson, M. Newman, and M. Lardelli. 2020. "Brain Transcriptome Analysis Reveals Subtle Effects on Mitochondrial Function and Iron Homeostasis of Mutations in the SORL1 Gene Implicated in Early Onset Familial Alzheimer's Disease." *Molecular Brain* 13: 142.

Bellenguez, C., F. Küçükali, I. E. Jansen, et al. 2022. "New Insights Into the Genetic Etiology of Alzheimer's Disease and Related Dementias." *Nature Genetics* 54: 412–436.

Bennett, D. A., J. A. Schneider, A. S. Buchman, L. L. Barnes, P. A. Boyle, and R. S. Wilson. 2012. "Overview and Findings From the Rush Memory and Aging Project." *Current Alzheimer Research* 9: 646–663.

Bersuker, K., J. M. Hendricks, Z. Li, et al. 2019. "The CoQ Oxidoreductase FSP1 Acts Parallel to GPX4 to Inhibit Ferroptosis." *Nature* 575: 688–692.

Beurskens, D. M., J. P. Huckriede, R. Schrijver, H. C. Hemker, C. P. Reutelingsperger, and G. A. Nicolaes. 2020. "The Anticoagulant and Nonanticoagulant Properties of Heparin." *Thrombosis and Haemostasis* 120: 1371–1383.

Bota, D. A., and K. J. A. Davies. 2002. "Lon Protease Preferentially Degrades Oxidized Mitochondrial Aconitase by an ATP-Stimulated Mechanism." *Nature Cell Biology* 4: 674–680.

Breen, D. P., R. Vuono, U. Nawarathna, et al. 2014. "Sleep and Circadian Rhythm Regulation in Early Parkinson Disease." *JAMA Neurology* 71: 589–595.

Brown, M. B. 1975. "400: A Method for Combining Non-independent, One-Sided Tests of Significance." *Biometrics* 31: 987–992.

Bulik-Sullivan, B. K., P.-R. Loh, H. K. Finucane, et al. 2015. "LD Score Regression Distinguishes Confounding From Polygenicity in Genome-Wide Association Studies." *Nature Genetics* 47: 291–295.

Caglayan, S., S. Takagi-Niidome, F. Liao, et al. 2014. "Lysosomal Sorting of Amyloid-β by the SORLA Receptor Is Impaired by a Familial Alzheimer's Disease Mutation." *Science Translational Medicine* 6: 223ra220.

Cai, T., H. Hirai, G. Zhang, et al. 2011. "Deletion of Ia-2 and/or Ia-2β in Mice Decreases Insulin Secretion by Reducing the Number of Dense Core Vesicles." *Diabetologia* 54: 2347–2357.

Cai, Y., S. Liu, R. B. Sothern, S. Xu, and P. Chan. 2010. "Expression of Clock Genes Per1 and Bmal1 in Total Leukocytes in Health and Parkinson's Disease." *European Journal of Neurology* 17: 550–554.

Carocci, A., A. Catalano, M. S. Sinicropi, and G. Genchi. 2018. "Oxidative Stress and Neurodegeneration: The Involvement of Iron." *Biometals* 31: 715–735.

Casanova, F., Q. Tian, D. S. Williamson, et al. 2024. "MRI-Derived Brain Iron, Grey Matter Volume, and Risk of Dementia and Parkinson's Disease: Observational and Genetic Analysis in the UK Biobank Cohort." *Neurobiology of Disease* 197: 106539.

Chen, B., X. Wen, H. Jiang, J. Wang, N. Song, and J. Xie. 2019. "Interactions Between Iron and α-Synuclein Pathology in Parkinson's Disease." *Free Radical Biology and Medicine* 141: 253–260.

Chen, L., C. Wang, X. Chen, et al. 2024. "GOLPH3 Inhibits Erastin-Induced Ferroptosis in Colorectal Cancer Cells." *Cell Biology International* 48: 1198–1211.

Cheng, W.-W., Q. Zhu, and H.-Y. Zhang. 2019. "Mineral Nutrition and the Risk of Chronic Diseases: A Mendelian Randomization Study." *Nutrients* 11: 378.

Cinar, O., and W. Viechtbauer. 2022. "The Poolr Package for Combining Independent and Dependent p Values." *Journal of Statistical Software* 101: 1–42.

Conchon, S., X. Cao, C. Barlowe, and H. R. Pelham. 1999. "Got1p and Sft2p: Membrane Proteins Involved in Traffic to the Golgi Complex." *EMBO Journal* 18: 3934–3946.

Cronin, P., M. J. McCarthy, A. S. P. Lim, et al. 2017. "Circadian Alterations During Early Stages of Alzheimer's Disease Are Associated

With Aberrant Cycles of DNA Methylation in BMAL1." *Alzheimers Dement* 13: 689–700.

Daniel, T., H. M. Faruq, J. Laura Magdalena, G. Manuela, and L. Christopher Horst. 2020. "Role of GSH and Iron-Sulfur Glutaredoxins in Iron Metabolism—Review." *Molecules* 25: 3860.

Dansie, L. E., S. Reeves, K. Miller, et al. 2014. "Physiological Roles of the Pantothenate Kinases." *Biochemical Society Transactions* 42: 1033–1036.

De Gassart, A., V. Camosseto, J. Thibodeau, et al. 2008. "MHC Class II Stabilization at the Surface of Human Dendritic Cells Is the Result of Maturation-Dependent MARCH I Down-Regulation." *Proceedings of the National Academy of Sciences of the United States of America* 105: 3491–3496.

De Jager, P. L., Y. Ma, C. McCabe, et al. 2018. "A Multi-Omic Atlas of the Human Frontal Cortex for Aging and Alzheimer's Disease Research." *Scientific Data* 5: 180142.

De Jager, P. L., J. M. Shulman, L. B. Chibnik, et al. 2012. "A Genome-Wide Scan for Common Variants Affecting the Rate of Age-Related Cognitive Decline." *Neurobiology of Aging* 33, no. 1017: e1011–e1015.

De Jager, P. L., G. Srivastava, K. Lunnon, et al. 2014. "Alzheimer's Disease: Early Alterations in Brain DNA Methylation at ANK1, BIN1, RHBDF2 and Other Loci." *Nature Neuroscience* 17: 1156–1163.

de Leeuw, C. A., J. M. Mooij, T. Heskes, and D. Posthuma. 2015. "MAGMA: Generalized Gene-Set Analysis of GWAS Data." *PLoS Computational Biology* 11: e1004219.

Desuzinges-Mandon, E., O. Arnaud, L. Martinez, F. Huché, A. Di Pietro, and P. Falson. 2010. "ABCG2 Transports and Transfers Heme to Albumin Through Its Large Extracellular Loop." *Journal of Biological Chemistry* 285: 33123–33133.

Devos, D., J. Labreuche, O. Rascol, et al. 2022. "Trial of Deferiprone in Parkinson's Disease." *New England Journal of Medicine* 387: 2045–2055.

Di Meo, I., M. Carecchio, and V. Tiranti. 2019. "Inborn Errors of Coenzyme A Metabolism and Neurodegeneration." *Journal of Inherited Metabolic Disease* 42: 49–56.

Drecourt, A., J. Babdor, M. Dussiot, et al. 2018. "Impaired Transferrin Receptor Palmitoylation and Recycling in Neurodegeneration With Brain Iron Accumulation." *American Journal of Human Genetics* 102: 266–277.

Elliott, L. T., K. Sharp, F. Alfaro-Almagro, et al. 2018. "Genome-Wide Association Studies of Brain Imaging Phenotypes in UK Biobank." *Nature* 562: 210–216.

Elrod, J. W., and J. D. Molkentin. 2013. "Physiologic Functions of Cyclophilin D and the Mitochondrial Permeability Transition Pore." *Circulation Journal* 77: 1111–1122.

Ferreira, A., I. Royaux, J. Liu, et al. 2022. "The 3-O Sulfation of Heparan Sulfate Proteoglycans Contributes to the Cellular Internalization of Tau Aggregates." *BMC Molecular and Cell Biology* 23: 61.

Ficiarà, E., I. Stura, A. Vernone, F. Silvagno, R. Cavalli, and C. Guiot. 2024. "Iron Overload in Brain: Transport Mismatches, Microbleeding Events, and How Nanochelating Therapies May Counteract Their Effects." *International Journal of Molecular Sciences* 25: 2337.

Fjorback, A. W., and O. M. Andersen. 2012. "SorLA Is a Molecular Link for Retromer-Dependent Sorting of the Amyloid Precursor Protein." *Communicative & Integrative Biology* 5: 616–619.

Fotiadis, D., Y. Kanai, and M. Palacín. 2013. "The SLC3 and SLC7 Families of Amino Acid Transporters." *Molecular Aspects of Medicine* 34: 139–158.

Fujita, H., Y. Iwabu, K. Tokunaga, and Y. Tanaka. 2013. "Membrane-Associated RING-CH (MARCH) 8 Mediates the Ubiquitination and Lysosomal Degradation of the Transferrin Receptor." *Journal of Cell Science* 126: 2798–2809.

Galy, B., M. Conrad, and M. Muckenthaler. 2024. "Mechanisms Controlling Cellular and Systemic Iron Homeostasis." *Nature Reviews Molecular Cell Biology* 25: 133–155.

Ganz, T. 2013. "Systemic Iron Homeostasis." *Physiological Reviews* 93: 1721–1741.

Ghoussaini, M., E. Mountjoy, M. Carmona, et al. 2021. "Open Targets Genetics: Systematic Identification of Trait-Associated Genes Using Large-Scale Genetics and Functional Genomics." *Nucleic Acids Research* 49: D1311–d1320.

Gibellini, L., A. De Gaetano, M. Mandrioli, et al. 2020. "Chapter One—The biology of Lonp1: More than a mitochondrial protease." In *International Review of Cell and Molecular Biology*, edited by L. Galluzzi, vol. 354, 1–61. Cambridge, MA, USA: Academic Press.

Gill, D., B. Benyamin, L. S. P. Moore, et al. 2019. "Associations of Genetically Determined Iron Status Across the Phenome: A Mendelian Randomization Study." *PLoS Medicine* 16: e1002833.

Glerup, S., A. Nykjaer, and C. B. Vaegter. 2014. "Sortilins in Neurotrophic Factor Signaling." In *Neurotrophic Factors. Handbook of Experimental Pharmacology*, edited by G. Lewin and B. Carter, vol. 220. Berlin, Heidelberg: Springer.

Gong, L., J. Sun, and S. Cong. 2023. "Levels of Iron and Iron-Related Proteins in Alzheimer's Disease: A Systematic Review and Meta-Analysis." *Journal of Trace Elements in Medicine and Biology* 80: 127304.

Gong, N.-J., R. Dibb, M. Bulk, L. van der Weerd, and C. Liu. 2019. "Imaging Beta Amyloid Aggregation and Iron Accumulation in Alzheimer's Disease Using Quantitative Susceptibility Mapping MRI." *NeuroImage* 191: 176–185.

Goto, T., J. Matsuzawa, S. Iemura, T. Natsume, and H. Shibuya. 2016. "WDR26 Is a New Partner of Axin1 in the Canonical Wnt Signaling Pathway." *FEBS Letters* 590: 1291–1303.

GTEx Consortium. 2017. "Genetic Effects on Gene Expression Across Human Tissues." *Nature* 550: 204–213.

Guo, K., P. Lukacik, E. Papagrigoriou, et al. 2006. "Characterization of Human DHRS6, an Orphan Short Chain Dehydrogenase/Reductase Enzyme: A Novel, Cytosolic Type 2 R-Beta-Hydroxybutyrate Dehydrogenase." *Journal of Biological Chemistry* 281: 10291–10297.

Haass, N. K., M. Kartenbeck, and R. E. Leube. 1996. "Pantophysin Is a Ubiquitously Expressed Synaptophysin Homologue and Defines Constitutive Transport Vesicles." *Journal of Cell Biology* 134: 731–746.

Hentze, M. W., M. U. Muckenthaler, B. Galy, and C. Camaschella. 2010. "Two to Tango: Regulation of Mammalian Iron Metabolism." *Cell* 142: 24–38.

Hermey, G. 2009. "The Vps10p-Domain Receptor Family." *Cellular and Molecular Life Sciences* 66: 2677–2689.

Hogenesch, J. B., Y. Z. Gu, S. Jain, and C. A. Bradfield. 1998. "The Basic-Helix-Loop-Helix-PAS Orphan MOP3 Forms Transcriptionally Active Complexes With Circadian and Hypoxia Factors." *Proceedings of the National Academy of Sciences of the United States of America* 95: 5474–5479.

Horn, T., K. Reddy Kakularam, M. Anton, C. Richter, P. Reddanna, and H. Kuhn. 2013. "Functional Characterization of Genetic Enzyme Variations in Human Lipoxygenases." *Redox Biology* 1: 566–577.

Hulme, B., A. Didikoglu, S. Bradburn, et al. 2020. "Epigenetic Regulation of BMAL1 With Sleep Disturbances and Alzheimer's Disease." *Journal of Alzheimer's Disease* 77: 1783–1792.

Iacobazzi, V., F. Palmieri, M. J. Runswick, and J. E. Walker. 1992. "Sequences of the Human and Bovine Genes for the Mitochondrial 2-Oxoglutarate Carrier." *DNA Sequence* 3: 79–88.

International Multiple Sclerosis Genetics Consortium, ANZgene, IIBDGC, and WTCCC2. 2019. "Multiple Sclerosis Genomic Map

Implicates Peripheral Immune Cells and Microglia in Susceptibility." *Science* 365, no. 6460: eaav7188.

Ivan, M., and W. G. Kaelin. 2017. "The EGLN-HIF O2-Sensing System: Multiple Inputs and Feedbacks." *Molecular Cell* 66: 772–779.

Jansen, I., J. Savage, K. Watanabe, et al. 2019. "Genome-Wide Meta-Analysis Identifies New Loci and Functional Pathways Influencing Alzheimer's Disease Risk." *Nature Genetics* 51, no. 3: 404–413. https://doi.org/10.1038/s41588-018-0311-9.

Jiang, X., K. Liu, H. Jiang, et al. 2023. "SLC7A14 Imports GABA to Lysosomes and Impairs Hepatic Insulin Sensitivity via Inhibiting mTORC2." *Cell Reports* 42: 111984.

Jiménez-Jiménez, F. J., H. Alonso-Navarro, E. García-Martín, and J. A. G. Agúndez. 2021. "Biological Fluid Levels of Iron and Iron-Related Proteins in Parkinson's Disease: Review and Meta-Analysis." *European Journal of Neurology* 28: 1041–1055.

Kanamori, Y., M. Sugiyama, O. Hashimoto, M. Murakami, T. Matsui, and M. Funaba. 2016. "Regulation of Hepcidin Expression by Inflammation-Induced Activin B." *Scientific Reports* 6: 38702.

Kane, L. A., M. Lazarou, A. I. Fogel, et al. 2014. "PINK1 Phosphorylates Ubiquitin to Activate Parkin E3 Ubiquitin Ligase Activity." *Journal of Cell Biology* 205: 143–153.

Kang, H. J., Y. I. Kawasawa, F. Cheng, et al. 2011. "Spatio-Temporal Transcriptome of the Human Brain." *Nature* 478: 483–489.

Kang, R., Y. Xie, H. J. Zeh, D. J. Klionsky, and D. Tang. 2019. "Mitochondrial Quality Control Mediated by PINK1 and PRKN: Links to Iron Metabolism and Tumor Immunity." *Autophagy* 15: 172–173.

Ke, Y., and Z. M. Qian. 2007. "Brain Iron Metabolism: Neurobiology and Neurochemistry." *Progress in Neurobiology* 83: 149–173.

Kelemen, M., E. Vigorito, L. Fachal, C. A. Anderson, and C. Wallace. 2024. "shaPRS: Leveraging Shared Genetic Effects Across Traits or Ancestries Improves Accuracy of Polygenic Scores." *American Journal of Human Genetics* 111: 1006–1017.

Kent, W. J., C. W. Sugnet, T. S. Furey, et al. 2002. "The Human Genome Browser at UCSC." *Genome Research* 12: 996–1006.

Kim, J. J., D. Vitale, D. V. Otani, et al. 2024. "Multi-Ancestry Genome-Wide Association Meta-Analysis of Parkinson's Disease." *Nature Genetics* 56: 27–36.

Kizuka, Y., Y. Tonoyama, and S. Oka. 2009. "Distinct Transport and Intracellular Activities of Two GlcAT-P Isoforms." *Journal of Biological Chemistry* 284: 9247–9256.

Klein, H.-U., C. McCabe, E. Gjoneska, et al. 2019. "Epigenome-Wide Study Uncovers Large-Scale Changes in Histone Acetylation Driven by Tau Pathology in Aging and Alzheimer's Human Brains." *Nature Neuroscience* 22: 37–46.

Kuhn, H., J. Barnett, D. Grunberger, et al. 1993. "Overexpression, Purification and Characterization of Human Recombinant 15-Lipoxygenase." *Biochimica et Biophysica Acta* 1169: 80–89.

Kühnle, A., R. Veelken, C. E. Galuska, et al. 2019. "Polysialic Acid Interacts With Lactoferrin and Supports Its Activity to Inhibit the Release of Neutrophil Extracellular Traps." *Carbohydrate Polymers* 208: 32–41.

Kung, W.-M., S.-P. Yuan, M.-S. Lin, et al. 2021. "Anemia and the Risk of Cognitive Impairment: An Updated Systematic Review and Meta-Analysis." *Brain Sciences* 11: 777.

Kunkle, B. W., B. Grenier-Boley, R. Sims, et al. 2019. "Genetic Meta-Analysis of Diagnosed Alzheimer's Disease Identifies New Risk Loci and Implicates Aβ, Tau, Immunity and Lipid Processing." *Nature Genetics* 51: 414–430.

Lambert, J. C., C. A. Ibrahim-Verbaas, D. Harold, et al. 2013. "Meta-Analysis of 74,046 Individuals Identifies 11 New Susceptibility Loci for Alzheimer's Disease." *Nature Genetics* 45: 1452–1458.

Lambert, J.-C., A. Ramirez, B. Grenier-Boley, and C. Bellenguez. 2023. "Step by Step: Towards a Better Understanding of the Genetic Architecture of Alzheimer's Disease." *Molecular Psychiatry* 28: 2716–2727.

Lande-Diner, L., C. Boyault, J. Y. Kim, and C. J. Weitz. 2013. "A Positive Feedback Loop Links Circadian Clock Factor CLOCK-BMAL1 to the Basic Transcriptional Machinery." *Proceedings of the National Academy of Sciences* 110: 16021–16026.

Landini, A., I. Trbojević-Akmačić, P. Navarro, et al. 2022. "Genetic Regulation of Post-Translational Modification of Two Distinct Proteins." *Nature Communications* 13: 1586.

Larsson, S. C., M. Traylor, R. Malik, M. Dichgans, S. Burgess, and H. S. Markus. 2017. "Modifiable Pathways in Alzheimer's Disease: Mendelian Randomisation Analysis." *British Medical Journal* 359: j5375.

Lawrence, R., T. Yabe, S. Hajmohammadi, et al. 2007. "The Principal Neuronal gD-Type 3-O-Sulfotransferases and Their Products in Central and Peripheral Nervous System Tissues." *Matrix Biology* 26: 442–455.

Layer, G., J. Reichelt, D. Jahn, and D. W. Heinz. 2010. "Structure and Function of Enzymes in Heme Biosynthesis." *Protein Science* 19: 1137–1161.

Lee, K.-M., I.-W. Hsu, and W.-Y. Tarn. 2010. "TRAP150 Activates Pre-mRNA Splicing and Promotes Nuclear mRNA Degradation." *Nucleic Acids Research* 38: 3340–3350.

Levi, S., M. Ripamonti, A. S. Moro, and A. Cozzi. 2024. "Iron imbalance in neurodegeneration." *Molecular Psychiatry* 29: 1139–1152.

Levi, S., and V. Tiranti. 2019. "Neurodegeneration With Brain Iron Accumulation Disorders: Valuable Models Aimed at Understanding the Pathogenesis of Iron Deposition." *Pharmaceuticals* 12: 27.

Li, Y.-Q., and C. Guo. 2021. "A Review on Lactoferrin and Central Nervous System Diseases." *Cells* 10: 1810.

Liberzon, A., C. Birger, H. Thorvaldsdóttir, M. Ghandi, J. P. Mesirov, and P. Tamayo. 2015. "The Molecular Signatures Database (MSigDB) Hallmark Gene Set Collection." *Cell Systems* 1: 417–425.

Liberzon, A., A. Subramanian, R. Pinchback, H. Thorvaldsdóttir, P. Tamayo, and J. P. Mesirov. 2011. "Molecular signatures database (MSigDB) 3.0." *Bioinformatics* 27: 1739–1740.

Liu, C., W. Li, K. A. Tong, K. W. Yeom, and S. Kuzminski. 2015. "Susceptibility-Weighted Imaging and Quantitative Susceptibility Mapping in the Brain." *Journal of Magnetic Resonance Imaging* 42: 23–41.

Liu, Y., N. Basty, B. Whitcher, et al. 2021. "Genetic Architecture of 11 Organ Traits Derived From Abdominal MRI Using Deep Learning." *eLife* 10: e65554.

Liu, Z., A. Ciocea, and L. Devireddy. 2014. "Endogenous Siderophore 2,5-Dihydroxybenzoic Acid Deficiency Promotes Anemia and Splenic Iron Overload in Mice." *Molecular and Cellular Biology* 34: 2533–2546.

Long, H.-Z., Y. Cheng, Z.-W. Zhou, H.-Y. Luo, D.-D. Wen, and L.-C. Gao. 2022. "The Key Roles of Organelles and Ferroptosis in Alzheimer's Disease." *Journal of Neuroscience Research* 100: 1257–1280.

Lu, B., S. Yadav, P. G. Shah, et al. 2007. "Roles for the Human ATP-Dependent Lon Protease in Mitochondrial DNA Maintenance." *Journal of Biological Chemistry* 282: 17363–17374.

Lu, L.-N., Z.-M. Qian, K.-C. Wu, W.-H. Yung, and Y. Ke. 2017. "Expression of Iron Transporters and Pathological Hallmarks of Parkinson's and Alzheimer's Diseases in the Brain of Young, Adult, and Aged Rats." *Molecular Neurobiology* 54: 5213–5224.

Lupton, M. K., B. Benyamin, P. Proitsi, et al. 2017. "No Genetic Overlap Between Circulating Iron Levels and Alzheimer's Disease." *Journal of Alzheimer's Disease* 59: 85–99.

Martin, M., P. Sandhu, R. Kumar, and N. J. Buchkovich. 2022. "The Immune-Specific E3 Ubiquitin Ligase MARCH1 Is Upregulated During Human Cytomegalovirus Infection to Regulate Iron Levels." *Journal of Virology* 96: e0180621.

Masaldan, S., A. I. Bush, D. Devos, A. S. Rolland, and C. Moreau. 2019. "Striking While the Iron Is Hot: Iron Metabolism and Ferroptosis in Neurodegeneration." *Free Radical Biology and Medicine* 133: 221–233.

Masson, P. L., J. F. Heremans, and E. Schonne. 1969. "Lactoferrin, an Iron-Binding Protein in Neutrophilic Leukocytes." *Journal of Experimental Medicine* 130: 643–658.

McCarthy, R. C., and D. J. Kosman. 2012. "Mechanistic Analysis of Iron Accumulation by Endothelial Cells of the BBB." *Biometals* 25: 665–675.

McCarthy, R. C., and D. J. Kosman. 2015. "Iron Transport Across the Blood–Brain Barrier: Development, Neurovascular Regulation and Cerebral Amyloid Angiopathy." *Cellular and Molecular Life Sciences* 72: 709–727.

McCarthy, R. C., Y. H. Park, and D. J. Kosman. 2014. "sAPP Modulates Iron Efflux From Brain Microvascular Endothelial Cells by Stabilizing the Ferrous Iron Exporter Ferroportin." *EMBO Reports* 15: 809-815-815.

McKenna, M. J., S. I. Sim, A. Ordureau, et al. 2020. "The Endoplasmic Reticulum P5A-ATPase Is a Transmembrane Helix Dislocase." *Science* 369: eabc5809.

Mignani, L., B. Gnutti, D. Zizioli, and D. Finazzi. 2021. "Coenzyme a Biochemistry: From Neurodevelopment to Neurodegeneration." *Brain Sciences* 11: 1031.

Mindler, K., E. Ostertag, and T. Stehle. 2021. "The Polyfunctional Polysialic Acid: A Structural View." *Carbohydrate Research* 507: 108376.

Moksnes, M. R., S. E. Graham, K.-H. Wu, et al. 2022. "Genome-Wide Meta-Analysis of Iron Status Biomarkers and the Effect of Iron on All-Cause Mortality in HUNT." *Communications Biology* 5: 591.

Mostafavi, S., C. Gaiteri, S. E. Sullivan, et al. 2018. "A Molecular Network of the Aging Human Brain Provides Insights Into the Pathology and Cognitive Decline of Alzheimer's Disease." *Nature Neuroscience* 21: 811–819.

Muñoz, Y., C. M. Carrasco, J. D. Campos, P. Aguirre, and M. T. Núñez. 2016. "Parkinson's Disease: The Mitochondria-Iron Link." *Parkinsons Dis* 2016: 7049108.

Nassan, M., and A. Videnovic. 2022. "Circadian Rhythms in Neurodegenerative Disorders." *Nature Reviews Neurology* 18: 7–24.

Ng, B., C. C. White, H.-U. Klein, et al. 2017. "An xQTL Map Integrates the Genetic Architecture of the Human brain's Transcriptome and Epigenome." *Nature Neuroscience* 20: 1418–1426.

Nguyen, T. P., A. Casarin, M. A. Desbats, et al. 2014. "Molecular Characterization of the Human COQ5 C-Methyltransferase in Coenzyme Q10 Biosynthesis." *Biochimica et Biophysica Acta* 1841: 1628–1638.

Nielsen, M. S., C. Gustafsen, P. Madsen, et al. 2007. "Sorting by the Cytoplasmic Domain of the Amyloid Precursor Protein Binding Receptor SorLA." *Molecular and Cellular Biology* 27: 6842–6851.

Nishimura, T., A. Kubosaki, Y. Ito, and A. L. Notkins. 2009. "Disturbances in the Secretion of Neurotransmitters in IA-2/IA-2β Null Mice: Changes in Behavior, Learning and Lifespan." *Neuroscience* 159: 427–437.

Nishizawa, H., M. Matsumoto, T. Shindo, et al. 2020. "Ferroptosis Is Controlled by the Coordinated Transcriptional Regulation of Glutathione and Labile Iron Metabolism by the Transcription Factor BACH1." *Journal of Biological Chemistry* 295: 69–82.

Oh, H. S.-H., J. Rutledge, D. Nachun, et al. 2023. "Organ Aging Signatures in the Plasma Proteome Track Health and Disease." *Nature* 624: 164–172.

Parker, J. L., J. C. Deme, D. Kolokouris, et al. 2021. "Molecular Basis for Redox Control by the Human Cystine/Glutamate Antiporter System xc()." *Nature Communications* 12: 7147.

Passemard, S., F. Perez, P. Gressens, and V. El Ghouzzi. 2019. "Endoplasmic Reticulum and Golgi Stress in Microcephaly." *Cell Stress* 3: 369–384.

Perry, S. C., C. Kalyanaraman, B. E. Tourdot, et al. 2020. "15-Lipoxygenase-1 Biosynthesis of 7S,14S-diHDHA Implicates 15-Lipoxygenase-2 in Biosynthesis of Resolvin D5." *Journal of Lipid Research* 61: 1087–1103.

Pesch, B., S. Casjens, D. Woitalla, et al. 2019. "Impairment of Motor Function Correlates With Neurometabolite and Brain Iron Alterations in Parkinson's Disease." *Cells* 8: 96.

Petit, F., A. Drecourt, M. Dussiot, et al. 2021. "Defective Palmitoylation of Transferrin Receptor Triggers Iron Overload in Friedreich Ataxia Fibroblasts." *Blood* 137: 2090–2102.

Poli, M., F. Anower-E-Khuda, M. Asperti, et al. 2019. "Hepatic Heparan Sulfate Is a Master Regulator of Hepcidin Expression and Iron Homeostasis in Human Hepatocytes and Mice." *Journal of Biological Chemistry* 294: 13292–13303.

Poli, M., D. Girelli, N. Campostrini, et al. 2011. "Heparin: A Potent Inhibitor of Hepcidin Expression In Vitro and In Vivo." *Blood* 117: 997–1004.

Pu, J., C. Schindler, R. Jia, M. Jarnik, P. Backlund, and J. S. Bonifacino. 2015. "BORC, a Multisubunit Complex That Regulates Lysosome Positioning." *Developmental Cell* 33: 176–188.

Purcell, S., B. Neale, K. Todd-Brown, et al. 2007. "PLINK: A Tool Set for Whole-Genome Association and Population-Based Linkage Analyses." *American Journal of Human Genetics* 81: 559–575.

Ramasamy, A., D. Trabzuni, S. Guelfi, et al. 2014. "Genetic Variability in the Regulation of Gene Expression in Ten Regions of the Human Brain." *Nature Neuroscience* 17: 1418–1428.

Ramírez-Peinado, S., T. I. Ignashkova, B. J. van Raam, et al. 2017. "TRAPPC13 Modulates Autophagy and the Response to Golgi Stress." *Journal of Cell Science* 130: 2251–2265.

Ridefelt, P., A. Larsson, J.-U. Rehman, and J. Axelsson. 2010. "Influences of Sleep and the Circadian Rhythm on Iron-Status Indices." *Clinical Biochemistry* 43: 1323–1328.

Ripamonti, M., P. Santambrogio, G. Racchetti, et al. 2022. "PKAN hiPS-Derived Astrocytes Show Impairment of Endosomal Trafficking: A Potential Mechanism Underlying Iron Accumulation." *Frontiers in Cellular Neuroscience* 16: 878103.

Rogers, J. T., and C. M. Cahill. 2020. "Iron-Responsive-Like Elements and Neurodegenerative Ferroptosis." *Learning & Memory* 27: 395–413.

Royle, S. J., N. A. Bright, and L. Lagnado. 2005. "Clathrin Is Required for the Function of the Mitotic Spindle." *Nature* 434: 1152–1157.

Rozani, V., N. Giladi, T. Gurevich, et al. 2019. "Anemia in Men and Increased Parkinson's Disease Risk: A Population-Based Large Scale Cohort Study." *Parkinsonism & Related Disorders* 64: 90–96.

Sanchez, M., B. Galy, B. Schwanhaeusser, et al. 2011. "Iron Regulatory Protein-1 and -2: Transcriptome-Wide Definition of Binding mRNAs and Shaping of the Cellular Proteome by Iron Regulatory Proteins." *Blood* 118: e168–e179.

Schenck, J. F. 1996. "The Role of Magnetic Susceptibility in Magnetic Resonance Imaging: MRI Magnetic Compatibility of the First and Second Kinds." *Medical Physics* 23: 815–850.

Sekine, Y., R. Houston, E. M. Eckl, et al. 2023. "A Mitochondrial Iron-Responsive Pathway Regulated by DELE1." *Molecular Cell* 83: 2059–2076. e2056.

Sepulveda-Diaz, J. E., S. M. Alavi Naini, M. B. Huynh, et al. 2015. "HS3ST2 Expression Is Critical for the Abnormal Phosphorylation of Tau in Alzheimer's Disease-Related Tau Pathology." *Brain* 138: 1339–1354.

Singh, N., S. Haldar, A. K. Tripathi, et al. 2014. "Brain Iron Homeostasis: From Molecular Mechanisms to Clinical Significance and Therapeutic Opportunities." *Antioxidants & Redox Signaling* 20: 1324–1363.

Singh, N. K., and G. N. Rao. 2019. "Emerging Role of 12/15-Lipoxygenase (ALOX15) in Human Pathologies." *Progress in Lipid Research* 73: 28–45.

Sloane, D. L., R. Leung, C. S. Craik, and E. Sigal. 1991. "A Primary Determinant for Lipoxygenase Positional Specificity." *Nature* 354: 149–152.

Snow, A. D., J. A. Cummings, and T. Lake. 2021. "The Unifying Hypothesis of Alzheimer's Disease: Heparan Sulfate Proteoglycans/Glycosaminoglycans Are Key as First Hypothesized Over 30 Years Ago." *Frontiers in Aging Neuroscience* 13: 710683. https://doi.org/10.3389/fnagi.2021.710683.

Sorokin, E. P., N. Basty, B. Whitcher, et al. 2022. "Analysis of MRI-Derived Spleen Iron in the UK Biobank Identifies Genetic Variation Linked to Iron Homeostasis and Hemolysis." *American Journal of Human Genetics* 109: 1092–1104.

Subramanian, A., P. Tamayo, V. K. Mootha, et al. 2005. "Gene Set Enrichment Analysis: A Knowledge-Based Approach for Interpreting Genome-Wide Expression Profiles." *Proceedings of the National Academy of Sciences of the United States of America* 102: 15545–15550.

Szklarczyk, D., A. L. Gable, K. C. Nastou, et al. 2021. "The STRING Database in 2021: Customizable Protein-Protein Networks, and Functional Characterization of User-Uploaded Gene/Measurement Sets." *Nucleic Acids Research* 49: D605–d612.

Ta, N., C. Qu, H. Wu, et al. 2022. "Mitochondrial Outer Membrane Protein FUNDC2 Promotes Ferroptosis and Contributes to Doxorubicin-Induced Cardiomyopathy." *Proceedings of the National Academy of Sciences of the United States of America* 119: e2117396119.

Tachiyama, R., D. Ishikawa, M. Matsumoto, et al. 2011. "Proteome of Ubiquitin/MVB Pathway: Possible Involvement of Iron-Induced Ubiquitylation of Transferrin Receptor in Lysosomal Degradation." *Genes to Cells* 16: 448–466.

Taira, K., H. Bujo, S. Hirayama, et al. 2001. "LR11, a Mosaic LDL Receptor Family Member, Mediates the Uptake of ApoE-Rich Lipoproteins In Vitro." *Arteriosclerosis, Thrombosis, and Vascular Biology* 21: 1501–1506.

Tamir, S., M. L. Paddock, M. Darash-Yahana-Baram, et al. 2015. "Structure–Function Analysis of NEET Proteins Uncovers Their Role as Key Regulators of Iron and ROS Homeostasis in Health and Disease." *Biochimica et Biophysica Acta* 1853: 1294–1315.

Teder, T., W. E. Boeglin, and A. R. Brash. 2014. "Lipoxygenase-Catalyzed Transformation of Epoxy Fatty Acids to Hydroxy-Endoperoxides: A Potential P450 and Lipoxygenase Interaction." *Journal of Lipid Research* 55: 2587–2596.

Telling, N. D., J. Everett, J. F. Collingwood, et al. 2017. "Iron Biochemistry Is Correlated With Amyloid Plaque Morphology in an Established Mouse Model of Alzheimer's Disease." *Cell Chemical Biology* 24: 1205–1215. e1203.

Teng, H., B. Wu, K. Zhao, G. Yang, L. Wu, and R. Wang. 2013. "Oxygen-Sensitive Mitochondrial Accumulation of Cystathionine β-Synthase Mediated by Lon Protease." *Proceedings of the National Academy of Sciences of the United States of America* 110: 12679–12684.

Tian, R., A. Abarientos, J. Hong, et al. 2021. "Genome-Wide CRISPRi/a Screens in Human Neurons Link Lysosomal Failure to Ferroptosis." *Nature Neuroscience* 24: 1020–1034.

Toki, T., J. Itoh, J. Kitazawa, et al. 1997. "Human Small Maf Proteins Form Heterodimers With CNC Family Transcription Factors and Recognize the NF-E2 Motif." *Oncogene* 14: 1901–1910.

Torii, S., N. Saito, A. Kawano, S. Zhao, T. Izumi, and T. Takeuchi. 2005. "Cytoplasmic Transport Signal Is Involved in Phogrin Targeting and Localization to Secretory Granules." *Traffic* 6: 1213–1224.

Tortorella, S., and T. C. Karagiannis. 2014. "Transferrin Receptor-Mediated Endocytosis: A Useful Target for Cancer Therapy." *Journal of Membrane Biology* 247: 291–307.

Treffry, A., Z. Zhao, M. A. Quail, J. R. Guest, and P. M. Harrison. 1997. "Dinuclear Center of Ferritin: Studies of Iron Binding and Oxidation Show Differences in the Two Iron Sites." *Biochemistry* 36: 432–441.

Trejo-Lopez, J. A., A. T. Yachnis, and S. Prokop. 2022. "Neuropathology of Alzheimer's Disease." *Neurotherapeutics* 19: 173–185.

Uchida, Y., K. Ito, S. Ohtsuki, Y. Kubo, T. Suzuki, and T. Terasaki. 2015. "Major Involvement of Na(+) -Dependent Multivitamin Transporter (SLC5A6/SMVT) in Uptake of Biotin and Pantothenic Acid by Human Brain Capillary Endothelial Cells." *Journal of Neurochemistry* 134: 97–112.

Uhlén, M., L. Fagerberg, B. M. Hallström, et al. 2015. "Proteomics. Tissue-Based Map of the Human Proteome." *Science* 347: 1260419.

Vallese, F., K. Kim, L. Y. Yen, et al. 2022. "Architecture of the Human Erythrocyte Ankyrin-1 Complex." *Nature Structural & Molecular Biology* 29: 706–718.

Vardarajan, B. N., Y. Zhang, J. H. Lee, et al. 2015. "Coding Mutations in SORL1 and Alzheimer Disease." *Annals of Neurology* 77: 215–227.

Vogt, A.-C. S., T. Arsiwala, M. Mohsen, M. Vogel, V. Manolova, and M. F. Bachmann. 2021. "On Iron Metabolism and Its Regulation." *International Journal of Molecular Sciences* 22: 4591.

Wakabayashi, S. 2013. "Chapter Nine - New Insights Into the Functions of Histidine-Rich Glycoprotein." In *International Review of Cell and Molecular Biology*, edited by K. W. Jeon, vol. 304, 467–493. Cambridge, MA, USA: Academic Press.

Wang, C., A. B. Martins-Bach, F. Alfaro-Almagro, et al. 2022. "Phenotypic and Genetic Associations of Quantitative Magnetic Susceptibility in UK Biobank Brain Imaging." *Nature Neuroscience* 25: 818–831.

Wang, C. Y., S. Jenkitkasemwong, S. Duarte, et al. 2012. "ZIP8 Is an Iron and Zinc Transporter Whose Cell-Surface Expression Is Up-Regulated by Cellular Iron Loading." *Journal of Biological Chemistry* 287: 34032–34043.

Wang, C.-Y., D. Meynard, and H. Y. Lin. 2014. "The Role of TMPRSS6/Matriptase-2 in Iron Regulation and Anemia." *Frontiers in Pharmacology* 5: 114.

Wang, D., S. Liu, J. Warrell, et al. 2018. "Comprehensive Functional Genomic Resource and Integrative Model for the Human Brain." *Science* 362: 6420. https://www.science.org/doi/epdf/10.1126/science.aat8464.

Wang, Z., L. Meng, L. Shen, and H.-F. Ji. 2020. "Impact of Modifiable Risk Factors on Alzheimer's Disease: A Two-Sample Mendelian Randomization Study." *Neurobiology of Aging* 91: 167.e111–167.e119.

Wang, Z., V. N. Patel, X. Song, et al. 2023. "Increased 3-O-Sulfated Heparan Sulfate in Alzheimer's Disease Brain Is Associated With Genetic Risk Gene HS3ST1." *Science Advances* 9: eadf6232.

Watanabe, K., E. Taskesen, A. van Bochoven, and D. Posthuma. 2017. "Functional Mapping and Annotation of Genetic Associations With FUMA." *Nature Communications* 8: 1826.

Watanabe, K., M. Umićević Mirkov, C. A. de Leeuw, M. P. van den Heuvel, and D. Posthuma. 2019. "Genetic Mapping of Cell Type Specificity for Complex Traits." *Nature Communications* 10: 3222.

Weger, B. D., C. Gobet, F. P. David, et al. 2021. "Systematic Analysis of Differential Rhythmic Liver Gene Expression Mediated by the Circadian Clock and Feeding Rhythms." *Proceedings of the National Academy of Sciences* 118: e2015803118.

Westra, H. J., M. J. Peters, T. Esko, et al. 2013. "Systematic Identification of Trans eQTLs as Putative Drivers of Known Disease Associations." *Nature Genetics* 45: 1238–1243.

Wiley, S. E., A. N. Murphy, S. A. Ross, P. van der Geer, and J. E. Dixon. 2007. "MitoNEET Is an Iron-Containing Outer Mitochondrial Membrane Protein That Regulates Oxidative Capacity." *Proceedings of the National Academy of Sciences of the United States of America* 104: 5318–5323.

Xu, D., and J. D. Esko. 2014. "Demystifying Heparan Sulfate-Protein Interactions." *Annual Review of Biochemistry* 83: 129–157.

Xu, J., Z. Wan, and B. Zhou. 2019. "Drosophila ZIP13 Is Posttranslationally Regulated by Iron-Mediated Stabilization." *Biochimica et Biophysica Acta, Molecular Cell Research* 1866: 1487–1497.

Yang, M., P. Chen, J. Liu, et al. 2019. "Clockophagy Is a Novel Selective Autophagy Process Favoring Ferroptosis." *Science Advances* 5: eaaw2238.

Ye, Y., Y. Shibata, C. Yun, D. Ron, and T. A. Rapoport. 2004. "A Membrane Protein Complex Mediates Retro-Translocation From the ER Lumen Into the Cytosol." *Nature* 429: 841–847.

Yien, Y. Y., and M. Perfetto. 2022. "Regulation of Heme Synthesis by Mitochondrial Homeostasis Proteins." *Frontiers in Cell and Developmental Biology* 10: 895521.

Yin, Z., Q. Liu, Y. Gao, et al. 2024. "GOLPH3 Promotes Tumor Malignancy via Inhibition of Ferroptosis by Upregulating SLC7A11 in Cholangiocarcinoma." *Molecular Carcinogenesis* 63: 912–925.

Yu, L., L. B. Chibnik, G. P. Srivastava, et al. 2015. "Association of Brain DNA Methylation in SORL1, ABCA7, HLA-DRB5, SLC24A4, and BIN1 With Pathological Diagnosis of Alzheimer Disease." *JAMA Neurology* 72: 15–24.

Zhang, J., Y. Zhang, J. Wang, et al. 2010. "Characterizing Iron Deposition in Parkinson's Disease Using Susceptibility-Weighted Imaging: An In Vivo MR Study." *Brain Research* 1330: 124–130.

Zhou, Y. F., X. M. Wu, G. Zhou, et al. 2018. "Cystathionine β-Synthase Is Required for Body Iron Homeostasis." *Hepatology* 67: 21–35.

Zhou, Z. D., and E.-K. Tan. 2017. "Iron Regulatory Protein (IRP)-iron Responsive Element (IRE) Signaling Pathway in Human Neurodegenerative Diseases." *Molecular Neurodegeneration* 12: 1–12.

Zulkefli, K. L., I. S. Mahmoud, N. A. Williamson, P. K. Gosavi, F. J. Houghton, and P. A. Gleeson. 2021. "A Role for Rab30 in Retrograde Trafficking and Maintenance of Endosome-TGN Organization." *Experimental Cell Research* 399: 112442.

Zuo, C.-Y., X.-Y. Hao, M.-J. Li, et al. 2024. "Anemia, Blood Cell Indices, Genetic Correlations, and Brain Structures: A Comprehensive Analysis of Roles in Parkinson's Disease Risk." *Parkinsonism & Related Disorders* 128: 107153.

Supporting Information

Additional supporting information can be found online in the Supporting Information section.